UNIVERSITY OF TROMSØ UIT

FACULTY OF SCIENCE
DEPARTMENT OF PHYSICS AND TECHNOLOGY

Rockslide Mapping in Norway by Means of Interferometric SAR Time Series Analysis

Tom Rune Lauknes

A dissertation for the degree of Philosophiae Doctor

December 2010

Abstract

Rockslides have a high socioeconomic and environmental importance in many countries. Norway is particularly susceptible to large rockslides due to its many fjords and steep mountains. One of the most dangerous hazards related to rock slope failures are tsunamis that can lead to large loss of life. It is therefore very important to systematically identify potential unstable rock slopes.

In this thesis, we consider the use of satellite remote sensing interferometric synthetic aperture radar (InSAR) for detecting surface displacement in rural areas of Norway. The main focus of the work has been on developing small baseline (SB) InSAR time series methods for *mapping* and *monitoring* of rockslides in Norway.

The first part of the thesis is a basic review of the satellite SAR imaging instrument, with a focus on the InSAR methodology. Different satellite sensors and their limitations is discussed. The introduction chapters have been written with the nonspecialist in mind.

In the second part of the thesis, we present a discussion about particular InSAR processing challenges in Norway, as well as preliminary results from two ongoing research projects, with the aim of demonstrating the possibilities that emerges by using new high-resolution SAR sensors, as well as the potential to perform regular surface displacement monitoring using radar corner reflectors.

Spatial phase unwrapping is a critical step for all InSAR processing, and two-dimensional unwrapping of sparse data sets is particularly challenging. We propose an L_1-norm-based SB InSAR time series approach that leads to better robustness with respect to phase unwrapping errors in the interferometric data stack.

It is well known that in mountainous regions, temporal variations in the stratified atmospheric refractive index profile will lead to a interferometric phase delay correlating to topography. We present a SB method for estimating and correcting the tropospheric stratification effect observed in a stack of SB interferograms.

The last chapters of the thesis demonstrate that InSAR is a powerful tool that can be used to identify the relative magnitude and spatial pattern of active rockslide sites on both a regional and individual rockslide site scale.

Acknowledgements

I owe my deepest gratitude to my team of supervisors: Torbjørn Eltoft from the University of Tromsø, Harald Johnsen and Yngvar Larsen from Norut, and John Dehls from the Geological Survey of Norway (NGU). I am grateful to you all for allowing me unrestricted freedom to pursue my own research ideas, and for providing knowledgeable guidance and tutoring when needed. Kjell Arild Høgda has been the project leader and my boss at Norut. I am thankful for his good-temper and never-ending patience, allowing me to focus on my thesis, even if other duties called. I am grateful to my colleagues at Norut for providing an excellent research environment.

I have had the opportunity to participate in fieldwork at several rockslide sites in Troms and at Åknes. In Troms, I have had the pleasure of joining researchers Iain Henderson, Tim Redfield, and Per Terje Osmundsen from NGU. I am grateful for their everlasting patience when trying to teach me concepts of field geology. I have many memorable experiences from the daily debriefings at *Blå Rock*. I am thankful to the crew from *Fjellskred i Troms* for their positive attitude to the InSAR monitoring project.

I am thankful to Lars Harald Blikra, Kjell Jogerud, and Tore Bergeng for supporting my work related to the Åknes/Tafjord rockslide monitoring project. The radar corner reflectors would not have been there without the skillful assistance of Åge Kjølås and Marc-Henri Derron. I thank Dan Johan Weydahl at Norwegian Defence Research Establishment (FFI) for being instrumental in initiating my PhD project.

Special thanks go to Howard Zebker for welcoming me to his research group at Stanford University during the academic year 2007/2008. I enjoyed the open collaborative style, and the weekly group meetings that provided a forum for stimulating discussions. I am further indebted to Piyush Shanker Agram for many interesting and fruitful discussions about everything from InSAR to cricket. I would also like to thank all other members of the lab for making my stay at Stanford a very memorable one.

I am grateful to Sean Buckley at Center for Space Research, University of Texas at Austin, for providing me with an undisturbed workplace during the period January 2010–June 2010. His hospitality was instrumental for the completion of this thesis.

I would like to thank the University of Tromsø for granting me the scholarship that made my research stay in California possible. The International Centre for Geohazards and NGU are acknowledged for cofunding my project. Satellite SAR data have been kindly provided by Kongsberg Satellite Services (KSAT) through an agreement with Norwegian Space Centre and the European Space Agency (ESA).

I am indebted to Anja Strømme in Menlo Park, California, for her unconditional hospitality when I needed a place to crash for a few days or weeks.

I thank all my friends for the good time I have had during the time of my study. I thank my family for supporting me throughout the years.

Last, but not least, I deeply thank Anna for all her patience, and for the good life we share.

Tom Rune Lauknes — Tromsø, 23rd December 2010.

Contents

Nomenclature

List of Acronyms

2D	two-dimensional
3D	three-dimensional
APS	atmospheric phase screen
ASAR	Advanced Synthetic Aperture Radar
DEM	digital elevation model
EM	electromagnetic
ERS	European Remote Sensing
ESA	European Space Agency
FM	frequency modulated
GB-InSAR	ground based interferometric SAR
GNSS	global navigation satellite system
GPS	global positioning system
InSAR	interferometric synthetic aperture radar
IRLS	iteratively reweighted least squares
LIDAR	light detection and ranging
LOS	line-of-sight
LS	least squares
ML	maximum likelihood
ML-PS	maximum likelihood persistent scatterer

NASA	National Aeronautics and Space Administration
PS	persistent scatterer
PSI	persistent scatterer interferometry
SAR	synthetic aperture radar
SB	small baseline
SBAS	small baseline subset algorithm
SLC	single-look complex
SNR	signal-to-noise ratio
ZTD	zenith total delay

Chapter 1

Introduction

This thesis is about differential interferometric synthetic aperture radar (InSAR) time series methods and their applications for land deformation monitoring. In this Chapter, we present the motivation for our study, and give an extended summary of the subsequent chapters of the thesis, including five journal publications. We conclude the Chapter by including a list of other international publications and presentations published by the author.

1.1 Motivation

Being a mountainous country, with long fjords and steep valley sides, Norway is particularly susceptible to large rock avalanches. In the last 100 years, over 170 people have been killed by tsunamis in fjords caused by large rock avalanches. In each case, the rock avalanche was preceded by many years of slow movement, with acceleration prior to slope failure [Ganerød et al., 2008, Eiken, 2008]. With several thousand kilometres of inhabited coastline and valleys, it is a challenge to identify similar hazards in an efficient manner. Once we suspect an area to be sliding, it may take several years of measurements to confirm it, and an extensive ground instrumentation to characterize the type of motion.

In order to fully understand the kinematics and geometric configurations susceptible for sliding, it is imperative to obtain precise measurements of the stability of potential unstable rock slopes. Traditionally, a discrete network of surface benchmarks have been installed and precisely levelled periodically. Lately, the use of global navigation satellite system (GNSS) monuments allows either periodical, or continuous measurements of surface motion. Other ground-based surveying techniques include robotic total stations, which measure distance and angle to a defined set of reflectors, and ground-based scanning light detection and ranging (LIDAR) systems. Furthermore, extensometers and tiltmeters can measure precise changes in an opening crack, and boreholes can be drilled in order to study the bedrock characteristics.

Common for all these approaches are that they produce sparse measurements (few

observations due to cost of establishing an observation network), and are often surveyed infrequently due to expensive infrastructure and logistics. In conclusion, *there is an obvious need for the development of remote sensing methods that regularly can measure surface stability over large areas.*

The InSAR remote sensing technique involves comparing the phase information from two ground-based, airborne, or spaceborne synthetic aperture radar (SAR) images, produced at different times, to potentially detect millimeter to centimeter scale ground deformation patterns. The first demonstration of the repeat-pass InSAR technique to detect surface displacement was presented by [Gabriel et al., 1989]. They used two National Aeronautics and Space Administration (NASA) SEASAT satellite SAR observations, separated by 12 days, to produce a ground surface displacement map relating the observed ground displacement to water absorbing clays.

Over the last decades, and in particular after the launch of the European Space Agency (ESA) European Remote Sensing (ERS) satellites in the 1990's, satellite based SAR interferometry has become an important tool for mapping topography, studying surface deformation, and observing glacial flows, see e.g. [Zebker and Goldstein, 1986, Massonnet et al., 1993, Goldstein et al., 1993, Massonnet et al., 1995, Massonnet and Feigl, 1998].

The interferometric phase measurements are, however, affected by various effects that can hamper operational surface displacement monitoring. The main limiting factors are atmospheric path delay that can introduce an unknown bias in the phase measurement [Zebker et al., 1997], and temporal decorrelation that makes InSAR phase measurements unreliable due to the change in relative position of the scatterers in a resolution element [Zebker and Villasenor, 1992]. These effects can to a certain degree be mitigated by combining multiple SAR observations using multi-temporal InSAR techniques. Using more than two SAR scenes can lead to redundant measurements, allowing for more advanced time series methods. The access to large historical SAR data archives, dating back to the early 1990's (ERS-satellites), have inspired the development of several innovative multi-temporal InSAR algorithms, e.g. [Ferretti et al., 2000, Ferretti et al., 2001, Berardino et al., 2002, Schmidt and Bürgmann, 2003, Werner et al., 2003, Hooper et al., 2004].

The motivation for this PhD project was to develop and improve time series InSAR algorithms, with the main purpose to actively use InSAR as a tool for rockslide mapping in Norway. The applicability of the small baseline subset algorithm (SBAS) [Berardino et al., 2002] to detect urban subsidence in Norway has already been demonstrated [Lauknes, 2004], and the use of the persistent scatterer interferometry (PSI) method for deformation mapping in rural terrain in northern Norway has been demonstrated by [Dehls et al., 2002]. However, relatively few InSAR studies in rural terrain have been performed.

The potential of InSAR to study landslides has been investigated by several authors, e.g. [Berardino et al., 2003, Hilley et al., 2004, Strozzi et al., 2005, Colesanti and Wasowski, 2006, Rott and Nagler, 2006]. Few of the studied areas are however directly comparable to typical conditions in northern Norway. The main challenges are long winter seasons,

limiting the total number of SAR scenes applicable for analysis and making temporal atmospheric filtering difficult, as well as constraining the deformation values that could be measured due to signal aliasing. Furthermore, the typical fjord landscape with steep mountains introduces large areas with low coherence, possibly introducing phase unwrapping ambiguities. The area with steep topography is also highly susceptible to InSAR atmospheric stratification effects [Hanssen, 2001].

1.2 Organization of the Thesis

This thesis consists of ten chapters, and is organized as follows. Chapters 2–3 contain an introduction to the topics of SAR and interferometric SAR, while Chapter 4 contains a description of the main study areas, as well as a discussion on particular InSAR processing challenges in Norway. We present preliminary results from two ongoing research projects, with the aim of demonstrating the possibilities that emerges by using new high-resolution SAR sensors, as well as the potential to perform continuous surface displacement monitoring using radar corner reflectors. Chapters 5–9 contains five manuscripts, forming the basis of this thesis. These are separately described in this subsection, where we summarize the main findings and highlight the original contribution of the author. Finally, Chapter 10 gives the conclusions, and points out future research directions.

Paper 1

T. R. Lauknes, H. A. Zebker, and Y. Larsen, **"InSAR Deformation Time Series Using an L_1-norm Small Baseline Approach,"** *IEEE Transactions on Geoscience and Remote Sensing*, doi:10.1109/TGRS.2010.2051951, 2010.

Spatial phase unwrapping is a critical step for all InSAR processing, and two-dimensional (2D) unwrapping of sparse data sets is particularly challenging. A typical interferogram is often divided into several sparsely distributed coherent areas, separated by large decorrelated areas such as e.g. water or vegetated areas. The decorrelated areas can introduce ambiguities for traditional 2D unwrapping methods, and unwrapping errors can lead to incorrectly estimated deformation time series when using time series InSAR methods.

In this paper, we propose an L_1-norm-based small baseline (SB) InSAR time series approach that leads to better robustness with respect to phase unwrapping errors in the interferometric data stack. It is well known that cost function minimization using L_1-norm is more robust than L_2-norm (least squares (LS)) if the data set has outlying points. Our method is based on the original SBAS method, and we implemented the L_1-norm based inversion using the iteratively reweighted least squares (IRLS) algorithm. In the paper, we show that the displacement phase of both synthetic data, as well as a real

data set that covers the San Francisco Bay area, is recovered more accurately than with L_2-norm solutions.

Paper 2

T. R. Lauknes, **"Atmospheric Stratification Delays in InSAR, Correction Using a Small Baseline Approach,"** *IEEE Geoscience and Remote Sensing Letters*, submitted, 2010.

Our main study areas are located along the Norwegian coastline, with typical fjord landscape with mountains that rise up to 2000 m above the Norwegian Sea. It is well known that in mountainous regions, temporal variations in the stratified refractive index profile will lead to a interferometric phase delay correlating with elevation [Delacourt et al., 1998,Hanssen, 2001,Doin et al., 2009]. This path delay can be misinterpreted as surface displacement, and correction is imperative. Mitigation of atmospheric stratification is therefore crucial to successfully apply InSAR for deformation mapping in areas with strong topography. Neither of the atmospheric filtering methods applied today in time series InSAR are optimized to handle temporally correlated atmospheric delay due to stratification.

The topic of this paper is mitigation of atmospheric stratification effects in time series InSAR. We present a SB method for estimating and correcting the tropospheric stratification observed in a stack of SB interferograms. We demonstrate the value of this approach using InSAR data from Envisat Advanced Synthetic Aperture Radar (ASAR), and compare the InSAR estimated delays with results from a global positioning system (GPS) network from the Åknes rockslide site in western Norway.

Paper 3

T. R. Lauknes, A. Piyush Shanker, J. F. Dehls, H. A. Zebker, I. H. C. Henderson, and Y. Larsen, **"Detailed rockslide mapping in northern Norway with small baseline and persistent scatterer interferometric SAR time series methods,"** *Remote Sensing of Environment*, vol. 114, no. 9, pp. 2097–2109, doi:10.1016/j.rse.2010.04.015, 2010.

In Norway, the arctic area of Lyngen is one area where rockslides cluster [Braathen et al., 2004, Blikra et al., 2006]. In this paper, we take the opportunity to apply both SBAS and PSI time series InSAR methods to study several known rockslides in this area. Due to the high latitude and arctic climate, vegetation above 600–700 m is scarce. This area is thus very suited for application of the InSAR methodology. Several different electromagnetic (EM) surface scattering mechanisms can be expected.

In this paper, we address the differences and similarities between the SB and the PSI multitemporal InSAR methods for displacement studies in rural terrain. The paper includes a short review of both the SBAS and the maximum likelihood persistent scatterer (ML-PS) implementation, as well as a discussion including the relevance of both

SB and PSI methods for analyzing the surface displacement in the study area.

Paper 4

I. H. C. Henderson, T. R. Lauknes, P. T. Osmundsen, J. Dehls, Y. Larsen, and T. F. Redfield, **"A structural, geomorphological and InSAR study of an active rock slope failure development,"** *Slope Tectonics*, Geological Society, London, Special Publications, 351, pp. 185–189, doi:10.1144/SP351.10, 2011.

Few studies of rockslides have addressed the relationships between structures, geomorphological expressions and direct evidence of movement. In this paper, we describe a case study where we combine time series InSAR with structural geology and geomorphology in the assessment of sliding processes on the Gámanjunni site in Troms County, northern Norway. We employ structural geology, geomorphology and the SB InSAR methodology to investigate the evolution of the surface features developed in response to movement of the Gámanjunni rockslide site.

In this paper, we show that the SB time series InSAR methodology provides a new method to measure the movement of potential rockslides, and thus provides a direct link between qualitative movement data and field observations. We document the relationship between variations in ground movement rates and changing back-scarp geomorphology at the Gámanjunni site as well as movement patterns within the incipient rockslide. We demonstrate that variations in InSAR detected movement velocity documents millimetre variations in scarp displacement and that this is reflected in the evolving back scarp geometry.

Tom Rune Lauknes collected the SAR data, carried out the InSAR analysis, participated in fieldwork, assisted in interpretation of the results, and contributed to writing of the manuscript.

Paper 5

P. T. Osmundsen, I. H. C. Henderson, T. R. Lauknes, Y. Larsen, T. Redfield, and J. Dehls, **"Active normal fault control on landscape and rock-slope failure in northern Norway,"** *Geology*, vol. 37, no. 2, pp. 135–138, doi:10.1130/G25208A.1, 2009.

In this paper, we apply a combination of structural, geomorphic, and InSAR surface displacement data to show that uplift of the northernmost onshore Scandinavian passive margin is associated with active normal faulting and anomalous clusters of landslides. We demonstrate that active normal faults control both landscape distribution and the clustering of rock-slope failures in the Lyngen area.

Tom Rune Lauknes collected the SAR data, carried out the InSAR analysis, participated in fieldwork, assisted in interpretation of the results, and contributed to writing of the manuscript.

1.3 Other Contributions by Author

During the course of the PhD research, the author has contributed to several publications and presentations, not included in the thesis.

Peer review

1. J. A. Reeves, R. Knight, H. A. Zebker, W. A. Schreüder, P. S. Agram, and **T. R. Lauknes**, "InSAR data links seasonal head change and aquifer parameters for an agricultural area in the San Luis Valley, Colorado," *Water Resources Research*, submitted, 2010.

2. P. T. Osmundsen, T. F. Redfield, B. H. W. Hendriks, S. Bergh, J. A. Hansen, I. H. C. Henderson, J. Dehls, **T. R. Lauknes**, Y. Larsen, E. Anda, and B. Davidsen, "Fault-controlled Alpine topography in Norway ," *Journal of the Geological Society of London*, Vol. 167, pp. 83–98, doi:10.1144/0016-76492009-019, 2010.

3. K. A. Høgda, R. Storvold, and **T. R. Lauknes**, "SAR Imaging of Glaciers," book chapter in *Remote Sensing of Glaciers: Techniques for Topographic, Spatial and Thematic Mapping of Glaciers*, P. Pellika and W. Gareth Rees (eds.), Taylor & Francis, pp. 153–178, 2009.

Other presentations

1. J. Reeves, R. Knight, H. A. Zebker, W. A. Schreüder, P. S. Agram, and **T. R. Lauknes**, "InSAR data produce specific storage estimates for an agricultural area in the San Luis Valley, Colorado," *American Geophysical Union Fall Meeting (AGU 2010)*, San Francisco, CA, U.S.A., December 13–17, 2010, presentation only.

2. **T. R. Lauknes**, Y. Larsen, E. Malnes, and H. H. Christiansen, "Permafrost monitoring using SAR and ground based techniques in Svalbard," *Third European Conference on Permafrost (EUCOP III)*, Longyearbyen, Svalbard, Norway, June 13–17, 2010, presentation only.

3. **T. R. Lauknes**, Y. Larsen, E. Malnes, and H. H. Christiansen, "Monitoring of periglacial landform changes in permafrost landscape using radar satellite time series," *ESA Living Planet Symposium 2010*, Bergen, Norway, June 28–July 2, 2010, presentation only.

4. **T. R. Lauknes**, Y. Larsen, and J. Dehls, "Mitigating InSAR phase delay due to tropospheric stratification using GPS and weather models, a corner reflector study," *ESA Living Planet Symposium 2010*, Bergen, Norway, June 28–July 2, 2010, presentation only.

5. **T. R. Lauknes**, J. Dehls, Y. Larsen, and L. H. Blikra, "Monitoring of the Åknes rockslide in Storfjorden, Western Norway using corner reflector InSAR," *6th International Workshop on SAR Interferometry: Advances in the Science and Applications of SAR Interferometry (FRINGE 2009)*, ESA ESRIN, Frascati, Italy, November 30–December 4, 2009, presentation only.

6. J. Dehls, Y. Larsen, **T. R. Lauknes**, and C. Froese, "Assessment of residual coal mine subsidence and riverbank stability in an urban setting using X-band and C-band PSI," *6th International Workshop on SAR Interferometry: Advances in the Science and Applications of SAR Interferometry (FRINGE 2009)*, ESA ESRIN, Frascati, Italy, November 30–December 4, 2009, presentation only.

7. Y. Larsen, **T. R. Lauknes**, E. Malnes, and H. H. Christiansen, "High-resolution InSAR analysis of Radarsat-2 Ultra-Fine mode and TerraSAR-X data for measuring fine-scale landscape changes due to permafrost activity," *6th International Workshop on SAR Interferometry: Advances in the Science and Applications of SAR Interferometry (FRINGE 2009)*, ESA ESRIN, Frascati, Italy, November 30–December 4, 2009, presentation only.

8. J. Reeves, R. Knight, H. A. Zebker, W. A. Schreüder, P. S. Agram, and **T. R. Lauknes**, "InSAR deformation time series for an agricultural area in the San Luis Valley," *Eos Trans. AGU, 90(22), Jt. Assem. Suppl., Abstract H13A-03*, 2009, presentation only.

9. C. Michoud, **T. R. Lauknes**, A. Pedrazzini, M. Jaboyedoff, R. Tapia, and G. Steinmann, "Differential Synthetic Aperture Radar Interferometry in monitoring large landslide (La Frasse, Switzerland)," *European Geosciences Union Annual Meeting (EGU 2009)*, Vienna, Austria, April 19–24, 2009, presentation only.

10. **T. R. Lauknes**, P. Shanker. A., and H. Zebker, "Multi-temporal InSAR analysis of landslides in Lyngen region, Norway," *American Geophysical Union Fall Meeting (AGU 2008)*, San Francisco, CA, U.S.A., December 15–19, 2008, presentation only.

11. **T. R. Lauknes**, P. Shanker. A., H. Zebker, and Y. Larsen, "A combined small baseline and persistent scatterer InSAR method for resolving land deformation in natural terrain," *33rd International Geological Congress (IGC33)*, Oslo, Norway, August 6–14, 2008, presentation only.

12. **T. R. Lauknes**, P. Shanker. A., H. Zebker, and Y. Larsen, "A combined small baseline and persistent scatterer InSAR method for resolving land deformation in natural terrain," *2008 IEEE International Geoscience & Remote Sensing Symposium (IGARSS)*, Boston, Massachusetts, U.S.A., July 6–11, 2008, presentation only.

13. **T. R. Lauknes**, P. Shanker. A., and H. Zebker, "A preliminary look at the Sichuan earthquake using ENVISAT ASAR interferometry," *2008 IEEE International Geo-*

science & Remote Sensing Symposium (IGARSS), Boston, Massachusetts, U.S.A., July 6–11, 2008, presentation only.

14. R. Freuenfelder, J. Tolgensbakk, H. Farbrot, **T. R. Lauknes**, "Rockglaciers in the Kåfjord Area, Troms, Northern Norway," *9th Internat. Conference on Permafrost*, Fairbanks, Alaska, U.S.A., June 29 - July 3, 2008.

15. J. F. Dehls, **T. R. Lauknes**, Y. Larsen, and I. H. C. Henderson, "Landslide mapping in northern Norway using SBAS InSAR," *European Geosciences Union Annual Meeting (EGU 2008)*, Vienna, Austria, April 13–18, 2008, presentation only.

16. P. T. Osmundsen, T. F. Redfield, B. Hendriks, I. Henderson, J. Dehls, **T. R. Lauknes**, O. Fredin, Y. Larsen, B. Davidsen, and E. Anda, "Normal fault control on alpine landscapes in Norway," *European Geosciences Union Annual Meeting (EGU 2008)*, Vienna, Austria, April 13–18, 2008, presentation only.

17. I. H. C. Henderson, **T. R. Lauknes**, P. T. Osmundsen, T. Redfield, and Y. Larsen, "The dynamics of active landslide development and evolution: a combined structural geology, geomorphology and InSAR approach," *Slope Tectonics 08*, Lausanne, Switzerland, February 15–16, 2008, presentation only.

18. P. T. Osmundsen, I. Henderson, **T. R. Lauknes**, T. F. Redfield, Y. Larsen, and J. Dehls, "Tectonic controls on topography and rockslide distribution in Troms county, Norway," *Slope Tectonics 08*, Lausanne, Switzerland, February 15–16, 2008, presentation only.

19. **T. R. Lauknes**, Y. Larsen, J. Dehls, I. Henderson, and H. A. Zebker, "Regional Landslide Mapping and Monitoring in Norway Using SBAS InSAR," *American Geophysical Union Fall Meeting (AGU 2007)*, San Francisco, CA, U.S.A., December 10–14, 2007, presentation only.

20. **T. R. Lauknes**, J. Dehls, L. H. Blikra, and Y. Larsen, "Rockslide hazards in Storfjorden, Western Norway - Application of InSAR and other site investigations," *5th International Workshop on ERS SAR Interferometry: Advances in SAR Interferometry from ENVISAT and ERS missions (FRINGE 2007)*, ESA ESRIN, Frascati, Italy, November 26–30, 2007, presentation only.

21. **T. R. Lauknes**, Y. Larsen, J. Dehls, I. Henderson, and H. A. Zebker, "Regional scale landslide mapping in Northern Norway using SBAS InSAR," *5th International Workshop on ERS SAR Interferometry: Advances in SAR Interferometry from ENVISAT and ERS missions (FRINGE 2007)*, ESA ESRIN, Frascati, Italy, November 26–30, 2007, presentation only.

22. **T. R. Lauknes**, Y. Larsen, H. Johnsen, and T. Eltoft, "Characterization of coherent scatterers in natural terrain using SAR polarimetry," in *Proc. 3rd International*

Workshop on Science and Applications of SAR Polarimetry and Polarimetric Interferometry (PolInSAR 2007), ESA ESRIN, Frascati, Italy, January 22–26, 2007, 6 pp.

23. I. H. Henderson, **T. R. Lauknes**, P. T. Osmundsen, T. Redfield, J. Dehls, and Y. Larsen, "The dynamics of active landslide development and evolution: a combined structural geology, geomorphology and InSAR approach," *American Geophysical Union Fall Meeting (AGU 2007)*, San Francisco, CA, U.S.A., December 10–14, 2007, presentation only.

24. H. H. Christiansen, I. Berthling, L. H. Blikra, J. Dehls, B. Etzelmĺler, H. Farbrot, O. Humlum, K. Isaksen, H. Juliussen, **T. R. Lauknes**, K. Midttømme, and J. S. Rønning, "Permafrost Observatory Project: A Contribution to the Thermal State of Permafrost in Norway and Svalbard, TSP NORWAY," *American Geophysical Union Fall Meeting (AGU 2007)*, San Francisco, CA, U.S.A., December 10–14, 2007, presentation only.

25. J. Dehls, **T. R. Lauknes**, Y. Larsen, and I. H. C. Henderson, "Regional landslide mapping and monitoring in Norway using SBAS InSAR," *3rd International Geohazards Workshop, IGOS Geohazards*, ESA ESRIN, Frascati, Italy, November 6–9, 2007, presentation only.

26. Y. Larsen, G. Engen, **T. R. Lauknes**, E. Malnes, and K. A. Høgda, "A generic differential InSAR processing system, with applications to land subsidence and SWE retrieval," in *Proc. Advances in SAR Interferometry from ENVISAT and ERS missions (FRINGE 2005)*, ESA ESRIN, Frascati, Italy, November 28–December 2, 6 pp., 2005.

Chapter 2

Synthetic Aperture Radar Imaging

In this Chapter, we will introduce the basic principles behind satellite synthetic aperture radar (SAR) imaging. More detailed treatments of the SAR principle can be found in e.g. [Curlander and McDonough, 1991, Franceschetti and Lanari, 1999, Cumming and Wong, 2005].

2.1 Synthetic Aperture Radar

A spaceborne or airborne SAR images the Earth's surface in a side-looking geometry as shown in Figure 2.1. As the SAR moves along its (assumed) straight path, it illuminates a *swath* on the ground by transmitting a series of EM microwave pulses. The angle between the radar beam and the surface normal is called *incidence angle*, θ.

The SAR receiver detects the stream of echoes reflected from the Earth's surface. The energy scattered back towards the radar is called *backscatter*, and the echoes are produced since the terrain consists of different *scatterers* such as, trees, rocks, or buildings on the ground that interacts with the incoming microwave radiation. The received signals, after demodulation, are *complex*, having both amplitude and phase. The received amplitude is characterized by geometrical properties of the scatterer, as well as geometrical imaging factors. The received phase is determined by the phase of the transmitted signal, the dielectric properties of the medium, and the position of the scatterer.

The SAR focused image, referred to as single-look complex (SLC), is arranged in a 2D array, with coordinates *slant range*, R, for the distance from the SAR, and *azimuth*, x, for the position of the scatterer along the SAR flight path, see Figure 2.1.

2.1.1 Range and azimuth resolution

A high signal-to-noise ratio (SNR) is desirable in all radar systems. The SAR focusing principle involves transmitting a linear frequency modulated (FM) chirped pulse, allowing the use of longer pulses to increase the pulse energy. If the bandwidth of the

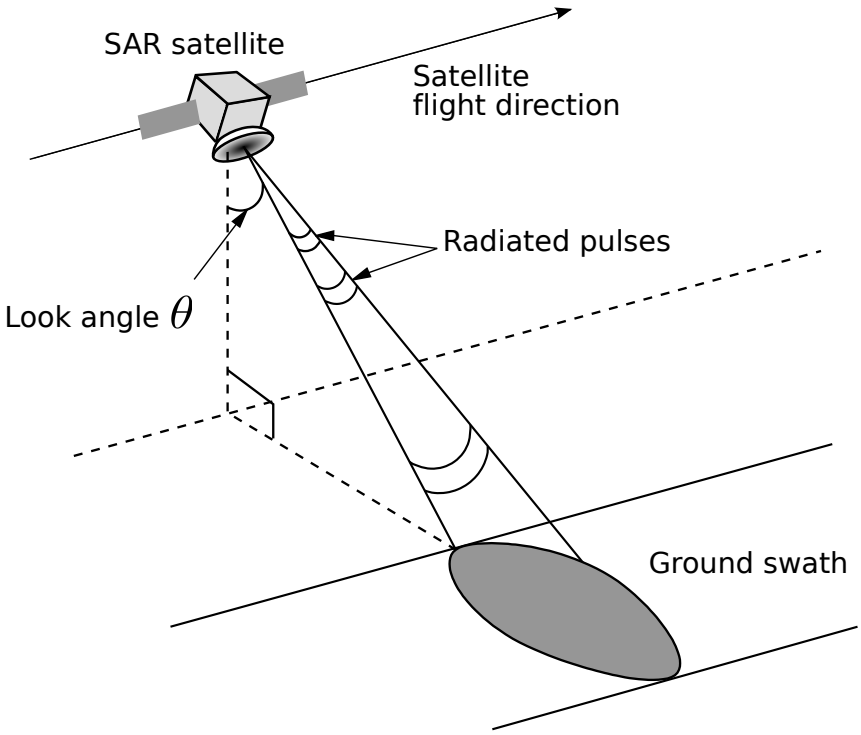

Figure 2.1: Simplified geometry of a synthetic aperture radar (SAR) system.

chirp is β [MHz], the slant range resolution is [Cumming and Wong, 2005]

$$\Delta R = \frac{c}{2\beta}, \tag{2.1}$$

where c is the velocity of light. For typical spaceborne SAR systems with pulse bandwidths from 15–150 MHz, this will result in a slant range resolution between 1–10 m.

Wiley showed in 1954 that a moving platform produces a Doppler shift, creating an azimuth frequency spread when passing over an object on the ground. Echoes reflected from objects in front of the moving sensor are frequency shifted relative to the echoes reflected from behind [Wiley, 1954]. This Doppler spread is in essence a motion-induced chirp, and a similar processing technique that is used in range can now also be employed in azimuth. The best azimuth resolution obtainable with a SAR is

$$\Delta x = \frac{L}{2}, \tag{2.2}$$

which is independent on the distance from the radar to the target [Franceschetti and Lanari, 1999]. Here, L is the antenna length in along-track direction. Shorter antennas yield finer resolutions since a single point on the ground will be illuminated for a longer time.

Table 2.1 summarizes the relevant satellite SAR sensors, with their important parameters.

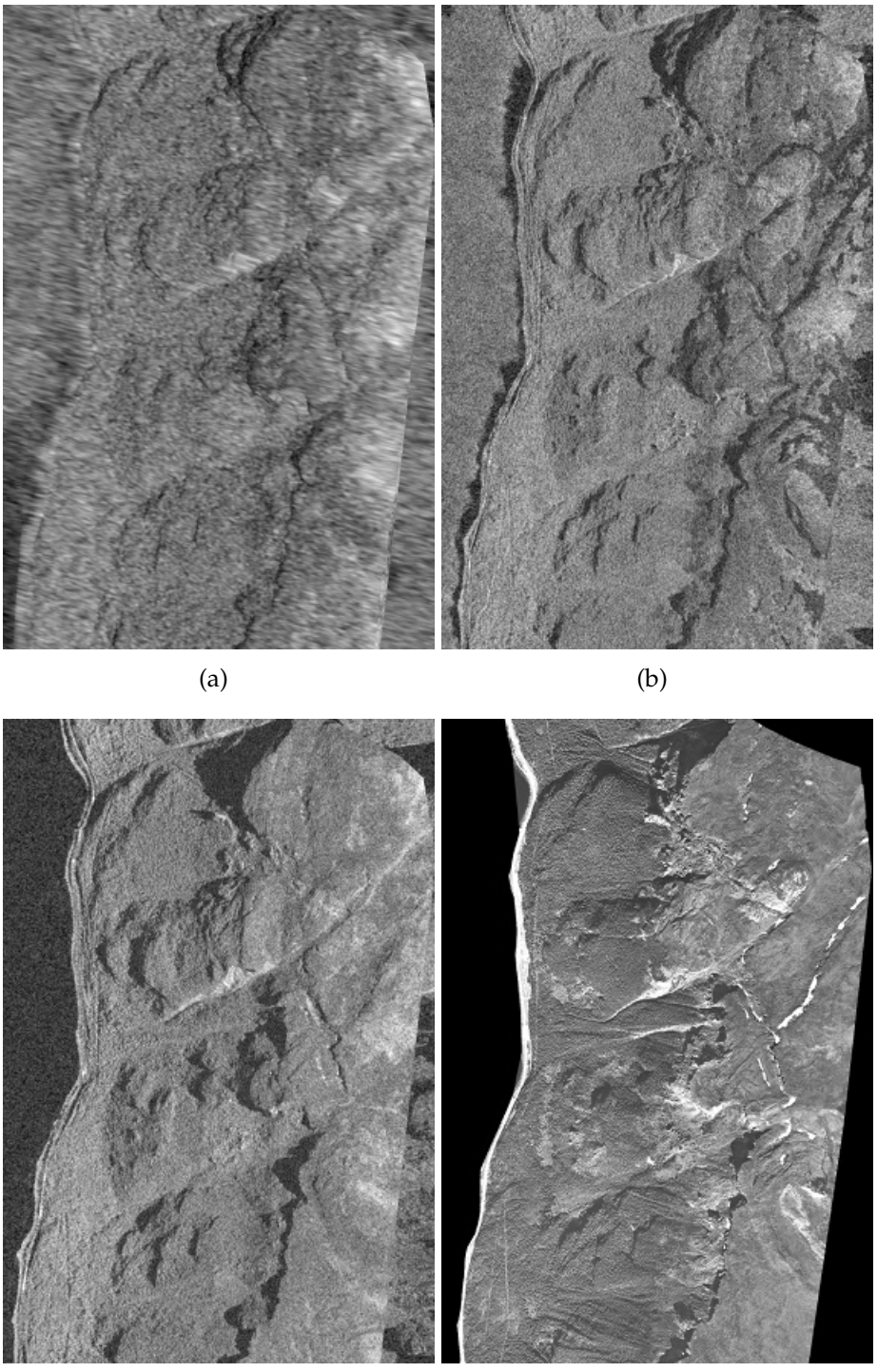

(a) (b)

(c) (d)

Figure 2.2: SAR images from different sensors illustrating different ground resolutions. All images have been geocoded to the same pixel size. (a) Envisat ASAR, (b) RADARSAT-2 Ultra-fine, (c) TerraSAR-X Stripmap. (d) aerial photo. It should be noted that the three SAR sensors operate with different incidence angles, leading to different levels of radar shadow.

Table 2.1: Relevant satellite SAR missions, with their important sensor parameters.

Mission	ERS-1/2	Envisat ASAR[a]	RADARSAT-1[a]	RADARSAT-2[a]
Country/Agency	ESA	ESA	Canada	Canada
Launch	1991/1995	2002	1995	2007
End of life	2000/2010[b]	2010[c]	2010[d]	2014
Frequency [GHz]	5.300	5.331	5.300	5.405
Wavelength [cm]	5.66	5.62	5.66	5.55
Polarization	VV	HH/VV + Alt.Pol.[e]	HH	HH, VV, HV, VH
Orbit Altitude [km]	780	800	798	798
Incidence Angle [deg]	21–26	20–50	20–50	20–50
Swath Width [km]	100	56–100	45–100	20–100
Ground range resolution [m]	20	12.5–28.0	7.8–26	3–25
Azimuth resolution [m]	5	5	8.4	3–28
Revisit Time [days]	35	35	24	24

[a] Only stripmap mode have been included.

[b] ERS-2 is operating without gyro since January 2001, affecting interferometric applications.

[c] The satellite orbit was changed October 22, 2010, ending the interferometric time series.

[d] Still operating.

[e] Alternating Polarization Mode (AP) gives two coregistered images per acquisition. HH/VV, HH/HV, or VV/VH polarization pairs possible.

2.2 SAR Geometrical Effects

The geometry of a SAR image is spanned by the range-azimuth coordinates. Due to the side-looking geometry, and related to the conversion of the measured slant range to the ground range, geometrical distortions will appear in the SAR image. The process of generating SAR images with *uniform* pixel sizes in a map projected coordinate system is called *geocoding*.

2.2.1 Ground range resolution

The resolution in (2.1) gives the minimum separation for two objects in the radar reference system. To obtain the *ground range resolution*, the slant range must be projected

Table 2.1: Relevant satellite SAR missions, with their important sensor parameters. (continued)

Mission	ALOS PALSAR[a]	TerraSAR-X[a]	COSMO-SkyMed[a]	Sentinel-1a/b[a]
Country/Agency	Japan	Germany	Italy	ESA
Launch	2005	2007	2007	2012
End of life	2010[d]	5 years	5 years[f]	7 years
Frequency [GHz]	1.27	9.65	9.6	5.405
Wavelength [cm]	23.60	3.10	3.12	5.55
Polarization	HH, VV, HV, VH	HH, VV, HV, VH	HH, VV, HV, VH	VV+VH, HH+HV
Orbit Altitude [km]	692	514	620	693
Incidence Angle [deg]	8–60	20–55	25–50	20–45
Swath Width [km]	30–70	5–30	10–40	80–400
Ground range resolution [m]	10–30	0.75–3.5	1–3	5–25
Azimuth resolution [m]	4.5	1.1–3.3	1–3	5–40
Revisit Time [days]	46	11	4[g]	12[h]

[a] Only spotlight and stripmap modes have been included.

[d] Still operating.

[f] Lifetime of each cluster satellite is 5 years, with a planned cluster operational period of 3 years.

[g] Cluster of four satellites with a theoretical 4 days revisit time.

[h] With the addition of Sentinel-1b, the revisit time will be 6 days.

onto the ground, see Figure 2.1

$$\Delta R_{\mathrm{g}} = \frac{\Delta R}{\sin\theta} = \frac{c}{2\beta\sin\theta}, \tag{2.3}$$

where β is the radar bandwidth, ΔR is the slant range resolution from (2.1), and θ is the radar incidence angle, as observed in Figure 2.1. The increase of the incidence angle θ from near to far range leads to an improvement in the ground resolution. For the ERS satellites, with a relatively steep incidence angle of $21°$–$26°$, this corresponds to an improvement in the ground range resolution from near range to far range.

Figure 2.2 shows examples of SAR images with different resolutions, including Envisat ASAR (5 m $\times$ 25 m), RADARSAT-2 Ultra-fine (1.6 m $\times$ 2.8 m), and TerraSAR-X Stripmap mode (1.0 m $\times$ 3.3 m), where the resolutions are given in (slant) range and azimuth directions, respectively. The improvement in distinguishable features is obvious.

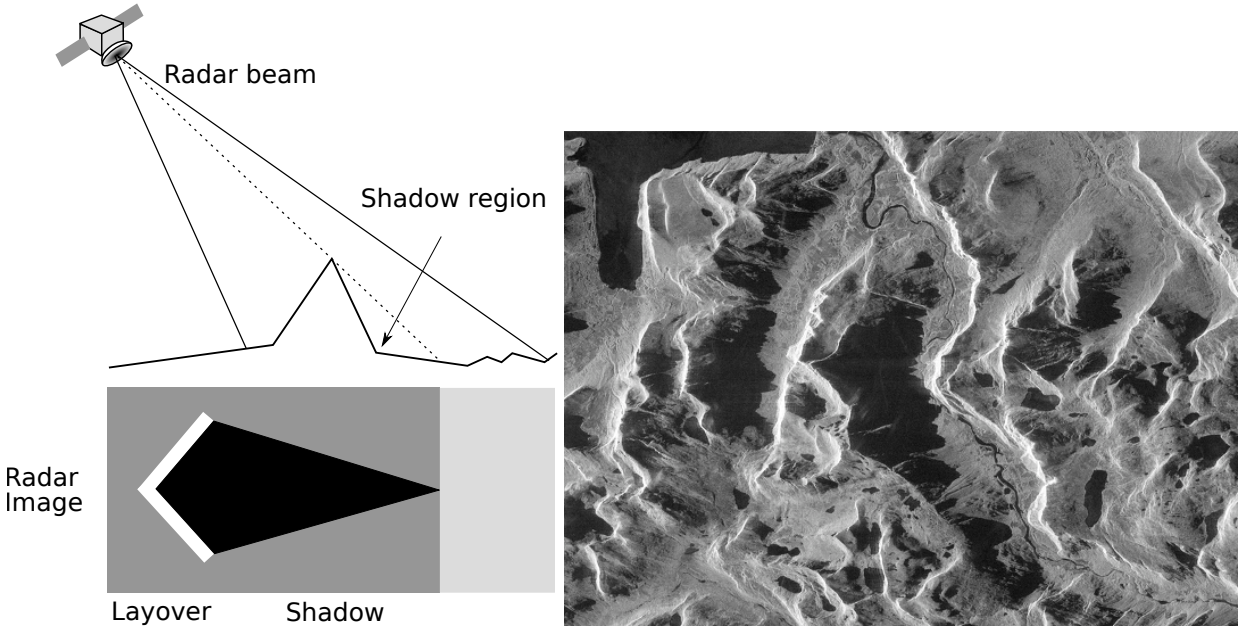

Figure 2.3: Example illustrating geometrical imaging effects that can limit SAR applications in mountainous regions. (a) geometrical principles behind radar *layover* and *shadow*, (b) a SAR intensity image covering the area of Romsdalen in Norway. Areas with severe layover and shadow can be seen.

2.2.2 Radar shadow and foreshortening

When topographic features exist, *foreshortening* can appear on the front side of a hill, resulting in compressed pixels on the ground. For steep-looking spaceborne radar systems, the across-track slant range differences between two points located on foreslopes of mountains are smaller than they would be in flat areas. In the extreme case, *layover* appear when the top of a hill is closer to the radar than the foot of the hill. In this case, the received signal from at least two different altitudes is added into one slant range resolution cell, leading to a very high radar return. The layover effect can easily be observed in SAR images as areas with extremely high intensity. On the other side of the mountain, radar *shadow* occurs in the area not being illuminated. In mountainous areas, foreshortening, layover, and shadow effects are obvious, see Figure 2.3 for an extreme example from the area of Romsdalen in Norway. Most modern satellites have the possibility to operate within a range of different incidence angles, while the ERS satellites, for example, had a fixed, relatively steep, incidence angle.

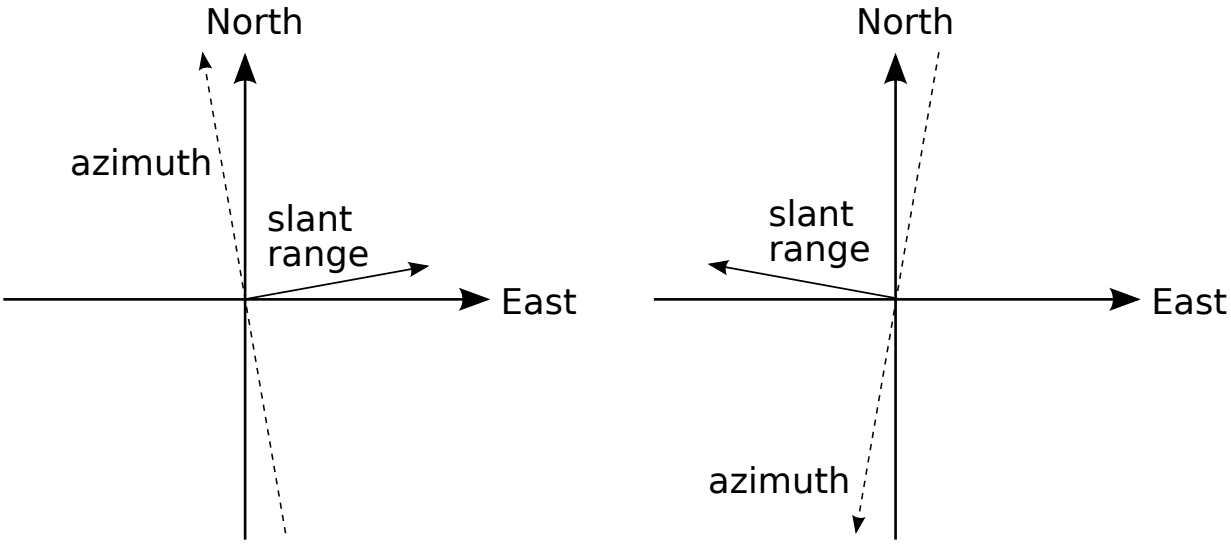

Figure 2.4: Geometry of ascending (left) and descending (right) satellite orbits.

2.3 Satellite Orbit Configuration

A polar orbiting satellite passes any area in both *ascending* and *descending* modes. An ascending orbit is defined where the satellite crosses the equator going from south to north, and the descending orbit where the satellite crosses the equator going from north to south, see Figure 2.4.

From Figure 2.4 it is clear that a descending orbit gives mainly nondistorted coverage in west facing slopes, and an ascending orbit covers east facing slopes.

However, as we will return to in Chapter 3, we would at this point like to stress that the satellite SAR imaging geometry, shown in Figure 2.4, limits the applicability to perform surface displacement analysis in certain areas. The radar is only sensitive to displacement that has a component in the radar line-of-sight (LOS) direction. Sensitivity is thus very low in cases where the actual surface displacement vector is near perpendicular to the LOS. Earth observing satellites in polar orbits fly in a direction close to North-South direction, and the sensitivity to surface displacement in this plane is near zero.

Chapter 3

SAR Interferometry

In this Chapter, we will introduce the principles behind the InSAR method. More detailed InSAR treatments can be found in e.g. [Massonnet and Feigl, 1998, Bamler and Hartl, 1998, Franceschetti and Lanari, 1999, Rosen et al., 2000, Rocca et al., 2000, Hanssen, 2001, Kampes, 2006]. In Section 3.7, we introduce the concept of interferometric time series methods.

3.1 Introduction

SAR interferometry uses the phase difference between a target in two SAR images to characterize ground surface parameters. Due to the imaging geometry, InSAR provides sensitivity to both surface topography as well as possible surface displacement changes. The first example of using InSAR for topographic mapping was shown by [Graham, 1974], while the first practical results of observations performed with a dual antenna side-looking airborne radar was reported by [Zebker and Goldstein, 1986]. The first demonstration of the repeat-pass differential InSAR technique to detect surface displacement was presented by [Gabriel et al., 1989].

The differential InSAR technique involves removing the topographic phase contribution [Rosen et al., 2000]. The phase difference between two SAR images can then potentially be used to detect millimeter to centimeter scale ground deformation patterns.

The so called *repeat-pass* InSAR technique involves comparing SAR data acquired at repeated satellite (or airborne) orbits, providing the possibility to study phenomena related to temporal ground surface changes occurring between the acquisitions. The launch of the ESA ERS satellites in the 1990's triggered a lot of InSAR research activity, and numerous applications were demonstrated. In this period, InSAR was successfully used to study surface displacement due to e.g. glacier dynamics [Goldstein et al., 1993], volcano deformation [Massonnet et al., 1995, Amelung et al., 2000], and earthquakes [Massonnet et al., 1993, Massonnet and Feigl, 1998].

Recently, the potentiality of differential InSAR has been investigated to study land-

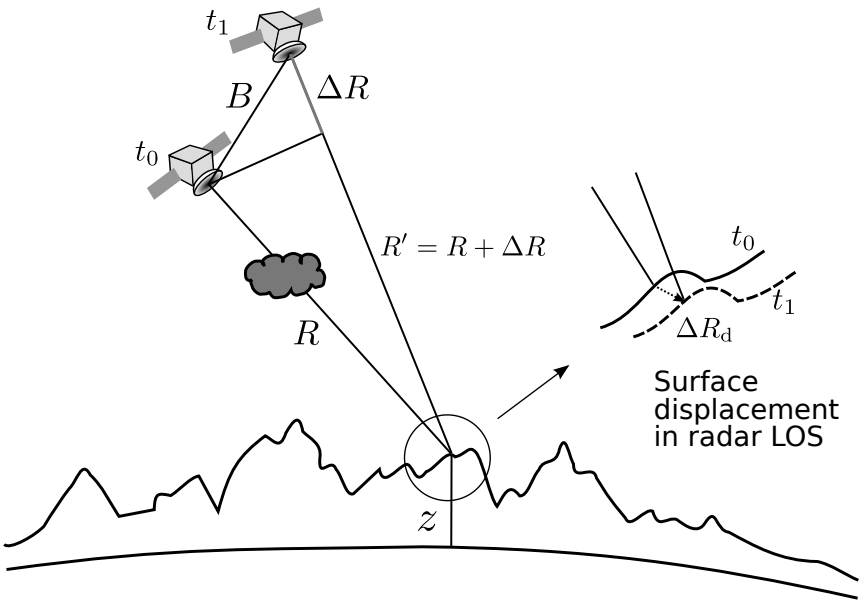

Figure 3.1: Detecting surface displacement with InSAR. An area on the ground is imaged at two different times t_0 and t_1. A possible surface deformation occurring between the acquisition times will lead to an interferometric phase term ΔR_{d}. The cloud at the t_0 radar acquisition illustrates that atmospheric effects can effect the radar propagation, producing an additional path delay.

slides and rockslides [Berardino et al., 2003, Hilley et al., 2004, Strozzi et al., 2005, Rott and Nagler, 2006, Colesanti and Wasowski, 2006].

3.2 Interferometric Phase

A coherent radar extracts information about a target by measuring both amplitude and phase of the received echo. The phase measured by a radar is a function of the two-way propagation delay, and is proportional to the distance to the target

$$\phi = \frac{4\pi}{\lambda} R, \tag{3.1}$$

where R is the geometrical distance travelled by the propagating EM wave.

Let us consider the InSAR configuration as shown in Figure 3.1, where an object on the ground at height z is imaged at two different times, $t = t_0$ and $t = t_1$. The two SAR antennas are separated by a baseline vector $\mathbf{B}$. The distances from the two antennas to the point on the ground are R and $R+\Delta R$. Each radar independently measures the time delay for the radar pulse to reach the point on the ground and return to the antenna.

The received amplitude and phase for a pixel on the ground in each of the two an-

tennas can then be written as

$$\begin{aligned} u_0 &= a_0 e^{-j\phi_0} = a_0 e^{-j\frac{4\pi}{\lambda}R} \\ u_1 &= a_1 e^{-j\phi_1} = a_1 e^{-j\frac{4\pi}{\lambda}(R+\Delta R)}, \end{aligned} \tag{3.2}$$

where a_0 and a_1 are the amplitudes of the two signals, j is the imaginary unit, and the received phase of each antenna is related to the target distance. From (3.2) we form the *complex interferogram* as

$$\Phi = u_0 u_1^* = a_0 a_1 e^{j\frac{4\pi}{\lambda}\Delta R} = a_0 a_1 e^{j\Delta\phi}, \tag{3.3}$$

where * denotes the complex conjugate, and $\Delta\phi$ is the *interferometric phase*. The path difference between the two signals can then be determined to an accuracy within a fraction of the wavelength by looking at the phase difference of the received echoes.

The observed phase in an interferogram ($\Delta\phi$) is thus related to the difference in distance to the target for the two acquisitions. The phase difference has several signal components: topography, terrain deformation in the radar line of sight (LOS) between the acquisitions, and atmospheric differences, as illustrated in Figure 3.1.

The interferometric phase difference, with respect to a ground reference point, can be decomposed into several parts [Berardino et al., 2002]

$$\Delta\phi = \frac{4\pi}{\lambda}\frac{B_\perp}{R\sin\theta}z + \frac{4\pi}{\lambda}\Delta R_d + \Delta\phi_{\mathrm{APS}} + \Delta\phi_{\mathrm{decorr}}, \tag{3.4}$$

where λ is the radar wavelength, z is the elevation of the target point above a reference plane, $B_\perp$ is the distance between the two orbits (perpendicular baseline), projected onto the LOS, ΔR_d is possible surface displacement in LOS, R is the range distance, θ is the incidence angle, $\Delta\phi_{\mathrm{APS}}$ is the difference in atmospheric path delay (atmospheric phase screen (APS)), and $\Delta\phi_{\mathrm{decorr}}$ is a noise term including other noise contributions.

In order to study surface displacement, the topographic contribution (first term of (3.4)) has to be removed. This is most often done by using an external high-precision digital elevation model (DEM) [Rosen et al., 2000]. However, a three-pass InSAR method can also be used. This method involves combining three SAR scenes; two with a short temporal baseline to retrieve the topographic signal, and the combination of these two with a third to produce a differential interferogram [Zebker et al., 1994].

InSAR is an extremely powerful technique for detection of surface displacement in the radar LOS direction. From Figure 3.1(right) it is clear that the interferometer measures the projection of the displacement vector in the radar LOS direction. In order to reconstruct the full three-dimensional (3D) vector displacement, several observations have to be made from different viewing angles.

3.3 Interferometric Coherence

The phase accuracy in SAR interferometry is mainly affected by phase noise and decorrelation. A quality measure of the interferometric phase is the complex correlation co-

efficient, or complex coherence, defined as [Bamler and Hartl, 1998]

$$\gamma = \frac{E[u_0 u_1^*]}{\sqrt{E[|u_0|^2]E[|u_1|^2]}}, \tag{3.5}$$

where $E[\cdot]$ is the expectation operator, and u_0 and u_1 are the two complex SAR image values. The expectation operators in (3.5) are often replaced with spatial averaging within a neighborhood of the pixel of interest. If we assume Gaussian image statistics, the maximum likelihood (ML) estimate of the coherence $|\gamma|$ is [Bamler and Hartl, 1998]

$$|\gamma|_{ML} = \frac{|\sum_{n=1}^{L} u_0[n]\, u_1^*[n]|}{\sqrt{\sum_{n=1}^{L} |u_0[n]|^2 \sum_{n=1}^{L} |u_1[n]|^2}}, \tag{3.6}$$

summing over L independent samples. Note that often only the magnitude value of the complex coherence, referred to as *coherence*, is used. The values of $|\gamma|$ are between 0 and 1, where a coherence value of 1 corresponds to perfect phase correlation between the two measurements. Coherence values less than unity correspond to reduced phase coherence, caused by noisy phase measurements.

3.4 Interferometric Phase Decorrelation

Phase decorrelation is due to changes in position of individual scatterers within the resolution cell [Zebker and Villasenor, 1992], and is one of the main limitations for successful use of InSAR. Decorrelation can arise from either SAR imaging geometric effects (spatial decorrelation), or from temporal backscattering changes (temporal decorrelation) [Gatelli et al., 1994, Zebker and Villasenor, 1992]. The different decorrelation sources contribute multiplicatively to the coherence γ, and the most important decorrelation sources can be written as [Zebker and Villasenor, 1992, Hanssen, 2001]

$$\gamma = \gamma^{\text{spatial}} \cdot \gamma^{\text{temporal}} \cdot \gamma^{\text{thermal}} \cdot \gamma^{\text{DopplerCentroid}} \cdot \gamma^{\text{volumetric}}. \tag{3.7}$$

Spatial baseline decorrelation occurs when the interferometric baseline is not exactly zero. The radar receives the coherent sum of all independent scatterers within the resolution cell, and these contributions are added slightly differently due to the different geometries. The baseline decorrelation is related to the different incidence angles of the two SAR acquisitions, and leads to a *critical baseline*[1] length, above which the interferometric phase is pure noise.

Temporal decorrelation is the most problematic to characterize theoretically. It is due to changes in geometrical or electrical properties of the surface, as function of time between the acquisitions. These changes may be caused by moving parts of vegetation, erosion on the land surface, or agricultural activity. Terrain containing variable liquid

[1] The critical baseline depends on pulse bandwidth, wavelength, and local topography.

water, such as e.g., areas covered with wet snow, will also have different scattering properties from one observation to the next [Guneriussen et al., 2001]. Forest is shown to have a generally low coherence, even for a temporal baseline as short as one day, while urban and arid areas show high coherence also for acquisition time intervals longer than one year [Strozzi et al., 2000]. The temporal decorrelation phenomena are dependent on the radar wavelength; longer wavelengths are less sensitive to small scale surface scattering changes, however with reduced sensitivity to displacement [Strozzi et al., 2003].

Thermal decorrelation is due to system noise, and can be related to the SNR, of the radar system, which for modern SAR sensors is close to unity [Hanssen, 2001]. Furthermore, decorrelation terms for the InSAR processing have not been included, since they only introduce small amounts of decorrelation [Hanssen, 2001].

Doppler centroid decorrelation is caused by the differences in Doppler centroids for the two acquisitions. It is the azimuth equivalent of the spatial decorrelation component, which is a range geometry phenomena.

Volumetric decorrelation is caused by propagation of the radar wave through the scattering medium. It depends highly on the radar wavelength and the dielectric properties in the medium.

3.5 Phase Unwrapping

Due to the complex SAR imaging process, the interferometric phase may only be measured on the restricted interval $[-\pi, \pi]$ (wrapped phase) [Bamler and Hartl, 1998]. A retrieval operation must therefore be carried out on the 2D measured InSAR phase field in order to estimate the phase gradient between two adjacent phase samples, and to relate it to any geophysical phenomenon [Goldstein et al., 1988]. The absolute unwrapped interferometric phase is directly proportional to the difference in path lengths for the SAR image pair. The process of restoring the correct multiple of 2π to each point of the interferometric phase image is referred to as *phase unwrapping*, and this step is one of the most challenging aspects for successful application of SAR interferometry.

Many different phase unwrapping algorithms exist, and the topic of 2D phase unwrapping is still one of the most challenging for operational use of InSAR. Some well-used phase unwrapping algorithms are discussed by [Goldstein et al., 1988, Bamler and Hartl, 1998, Costantini, 1998, Ghiglia and Pritt, 1998, Chen and Zebker, 2000, Chen and Zebker, 2001].

If we are interested in monitoring slow moving surface phenomena, e.g. rockslides, we need to apply many SAR scenes captured over a long period. Consequently, the interferogram stack will include interferograms formed using large temporal or spatial baselines. Thus, large areas will often decorrelate, due mainly to large spatial baselines and temporal effects that result from changes in scattering properties within the resolution cell between the two dates used to form the interferogram [Zebker and Villasenor, 1992, Hanssen and Usai, 1997]. Such decorrelation effects often contaminate large ar-

eas in the interferograms with phase noise, making the retrieval of absolute phase from measurements that are ambiguous by integer multiples of 2π, a very challenging task.

Access to large stacks of SAR data have led to the development of sparse space-time algorithms that try to exploit the redundant information in both space and time [Pepe and Lanari, 2006, Hooper and Zebker, 2007, Shanker and Zebker, 2010].

3.6 Electromagnetic Propagation Delay

The true refractivity of the atmosphere is different from vacuum, and any propagating electromagnetic waves will be delayed. The total atmospheric delay consists of two parts. The first part is related to the propagation velocity being lower than speed of light. The other part is related to signal bending, which is a result of refractive index variations both in the plane perpendicular to the propagation direction, and in the propagation direction [Ishimaru, 1978, Ulaby et al., 1982, Davis et al., 1985]. The bending delay is very small, and can be ignored for typical SAR systems.

Assuming a spherically symmetric atmosphere, the atmospheric zenith total delay (ZTD) through the atmosphere is found by integrating the refractivity $N(z)$ along the propagation path between the surface elevation z_0 and the top of the atmosphere z_∞

$$l = \int_{z_0}^{z_\infty} N(z)dz. \tag{3.8}$$

From 3.1, the total two-way phase delay measured by the radar is

$$\phi = \frac{4\pi}{\lambda}(R + l) = \frac{4\pi}{\lambda}[R + \int_{z_0}^{z_\infty} N(z)dz], \tag{3.9}$$

where R is the geometrical distance (in free space), and l is an equivalent distance due to the atmospheric path delay.

3.6.1 Tropospheric effects on InSAR measurements

An interferogram is a difference between two SAR acquisitions, and spatial or temporal changes of the refractivity modify the spatial propagation velocity of the electromagnetic wave. A radar interferometer measures the phase difference with accuracy on the order of a fraction of the wavelength; more than accurate enough to be influenced by atmospheric path delay. Phase propagation delay due to atmospheric variability is one of the main error sources in repeat-pass InSAR. It produces erroneous differential range delays that, if not corrected for, can be misinterpreted as either topography or displacement [Goldstein, 1995, Zebker et al., 1997]. At the microwave frequencies in use at the current operating SAR satellites (X-, L-, and C-band), phase delay caused by tropospheric precipitable water vapor can reach up to 10–20 cm [Goldstein, 1995, Zebker et al., 1997, Hanssen, 2001].

It is common to divide the atmospheric path delay into one component coming from turbulent mixing processes, and a stratified component correlating with elevation [Hanssen, 2001]. Turbulent mixing comes from mixing processes in the inhomogeneous atmosphere [Ishimaru, 1978], while stratification results from variations in the vertical refractive index profile [Hanssen, 2001].

Following [Hanssen, 2001,Doin et al., 2009], we separate the atmospheric refractivity into a component $\delta N(x, y, z)$ related to spatially variable, turbulent atmosphere, and one component $\bar{N}(z)$ related to a spatially averaged atmospheric stratification.

$$N(x, y, z) = \bar{N}(z) + \delta N(x, y, z), \tag{3.10}$$

where x, y are range and azimuth positions, and z is height above the ellipsoid.

The stratification effect on InSAR data can be severe in areas with rough topography, and the research topic has been the source of several investigations, focusing both on quantification and mitigation, e.g. [Goldstein, 1995,Beauducel et al., 2000,Bonforte et al., 2001, Wadge et al., 2002, Webley et al., 2002, Remy et al., 2003, Lohman and Simons, 2005,Cavalié et al., 2007,Chaabane et al., 2007,Doin et al., 2009].

In Chapter 6, we present an approach to estimate and mitigate stratification effects using a stack of small baseline SAR interferograms.

3.7 Time Series InSAR

The use of spaceborne InSAR for surface displacement studies had its breakthrough with the launch of the ESA ERS C-band (5.5 cm wavelength) satellites, and during the 1990's, the principle of differential InSAR to study different kinds of surface displacement phenomena was widely demonstrated [Massonnet and Feigl, 1998].

The challenge in InSAR is to separate the wanted signal (e.g. deformation or topography) from the sum of all phase contributions. For terrain displacement studies, temporal decorrelation can be considered a random noise source while errors in the DEM used to remove the topographic phase, orbital errors, and atmospheric changes will introduce a spatially correlated phase error contribution [Zebker and Villasenor, 1992,Zebker et al., 1997,Hanssen, 2001].

Later, the research community realized that C-band InSAR systems are very prone to temporal decorrelation, limiting the use of C-band radars for long-term surface displacement monitoring, particularly in areas with vegetation cover.

The general availability of historical SAR data for research use, has since the late 1990's led to the development of several innovative *time series* InSAR methods. By moving from single interferograms that can give information about a distinct deformation event (e.g. an earthquake), new methods are focusing on the studies of entire data stacks, composed of SAR data from many years, to study the *temporal displacement history*. Furthermore, the availability of large data stacks makes it possible to apply temporal and spatial filters to mitigate unwanted phase contributions.

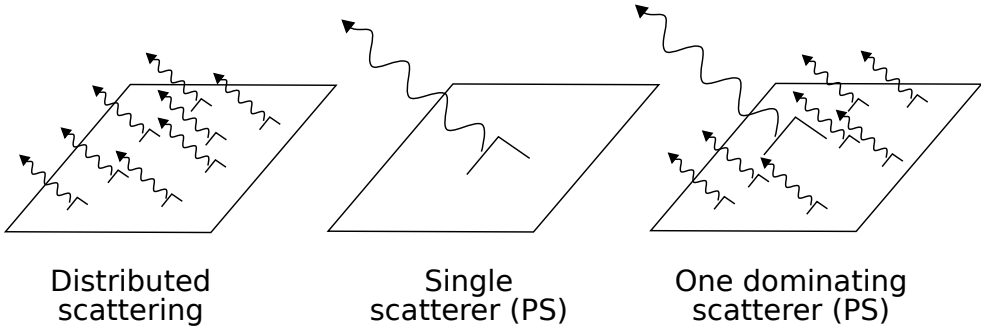

Figure 3.2: Different surface scattering mechanisms. A pixel with distributed scattering mechanism (left), a dominating point scatterer (middle), and a pixel with one scatterer that is brighter than all other (right). The images represent the scatterers contributing to the phase of a singe pixel. Modified from [Hooper et al., 2007].

The advanced time series InSAR methods can be broadly classified into two main groups:

- methods based on *spatial correlation* and distributed scattering, referred to as *small baseline* methods (SB) [Lundgren et al., 2001, Berardino et al., 2002, Mora et al., 2003, Schmidt and Bürgmann, 2003, Lanari et al., 2007, Prati et al., 2010, Sansosti et al., 2010], and
- methods based on locating persistent scatterers (PSs), referred to as persistent scatterer interferometry (PSI) methods [Ferretti et al., 2000, Ferretti et al., 2001, Werner et al., 2003, Hooper et al., 2004, Kampes, 2006, Prati et al., 2010].

A method combining both SB and PSI has been presented by [Hooper, 2008].

Figure 3.2 illustrates different scattering mechanisms that can be expected from a pixel under study. A coherent point like target is a scatterer that dominates the scattering from the resolution cell. Due to the broad scattering lobe, point targets are visible from a large span of viewing angles. A PS is a target whose amplitude and phase is constant as a function of time.

If a pixel includes one scatterer that is brighter than the other ones, the pixel phase variance is significantly reduced with respect to the case of distributed scattering from a high number of point targets. A persistent scatterer can be the corner of a building or a rock formation in rural areas.

The other scattering method illustrated in Figure 3.2 is distributed scattering, where the measured scattering is the coherent summation of all individual small scatterers within the resolution cell.

3.7.1 Small baseline methods

Small baseline methods are optimized for the distributed scattering mechanism, where several adjacent resolution cells represent the same physical deformation phenomena.

In areas with distributed scattering, *complex multilooking* is applied in order to reduce phase decorrelation noise [Zebker and Villasenor, 1992]. However, the cost of this averaging is a reduction of the spatial resolution.

Given a data stack of multiple SAR images, the distributed scattering method will give best results when exploiting interferometric pairs with as small spatial baseline as possible. The rationale behind all SB methods is to combine interferograms with a short spatial baseline, in order to minimize spatial decorrelation as well as effects due to errors in the DEM used.

The *stacking* approach is the simplest form of an SB approach. In this method, short baseline interferograms are averaged, weighted by the temporal difference between the scenes used, in order to provide a mean velocity displacement map, with reduced atmospheric noise [Sandwell and Price, 1998, Peltzer et al., 2001].

Later, other SB approaches have been presented, with SBAS as the most well known. Common to these SB methods is that they combine interferograms acquired with small baselines, to invert for displacement signatures, in addition to allowing for application of advanced atmospheric filters.

The SBAS method, one specific SB implementation, is described in more detail in chapters 5 and 7.

3.7.2 Persistent scatterer methods

The term persistent scatterer interferometry (PSI) characterizes InSAR techniques that analyze the temporal phase evolution of individual coherent point scatterers.

It was first noted by [Hanssen and Usai, 1997, Usai, 1997] that certain man made targets exhibited high coherence even when using interferograms with long time spans (temporal baseline) and large spatial baselines. It became clear that these point targets could be exploited for displacement monitoring.

The approach referred to in the literature as "Permanent Scatterer" or "Persistent Scatterer" has been developed by Politecnico di Milano (the Technical University of Milan) [Ferretti et al., 2000, Ferretti et al., 2001], and is based on analyzing a data stack of multiple SAR scenes (typically $>$20) in order to find pixels that contain a scatterer that is coherent over time. Differential interferograms are produced with respect to one common master geometry. All interferometric combinations are employed, even those exceeding the critical baseline. The generated interferograms are often severely decorrelated. However, by searching for pixels that include a stable scatterer, a network of so called *persistent scatterers* can be established, where displacement signal and 3D scatterer position can be resolved, even in areas where temporal and spatial decorrelation prevents the use of standard multilooking techniques. The persistent scatterers can be selected based on amplitude stability in the whole set of images. Such a statistical measure requires a large stack of images.

The persistent scatterer InSAR principle is not the main topic of this thesis. However, in Chapter 7, we present a study where SBAS and PSI methods are compared.

Chapter 4

Discussion

In this Chapter, we discuss particular challenges for successful application of InSAR in typical Norwegian fjord landscape. As a general comment, we observe that the rockslides in northern Norway are mostly located above 500–700 m elevation, where the vegetation cover is limited. Hence, the interferometric coherence is generally very good. However, as we will discuss in this Chapter, there are certain conditions that make InSAR processing challenging. In Section 4.3 we discuss the possibilities that emerges from using new high-resolution sensors, and in Section 4.4 we briefly discuss how we can move from mapping to monitoring by using radar corner reflectors.

4.1 Study Areas

In Norway, several counties are susceptible to large rockslides [Blikra et al., 2006]. A comprehensive study is currently ongoing, involving several different institutions and international partners, focusing on the possibility for large rockslides in Norway. The main focus areas has been Lyngen in Troms County and Møre og Romsdal County. These were chosen because of their steep topography and history of rockslide activity [Braathen et al., 2004, Blikra et al., 2006].

Two selected rockslides, *Åknes* in Møre og Romsdal County, western Norway, and *Nordnes* in Troms County, northern Norway, have been classified as high-risk due to their high consequence if a catastrophic failure would happen. These rockslides, illustrated in Figure 4.1, are the main study sites for the research in this thesis.

4.1.1 Åknes

The *Åknes* rockslide is located in Møre og Romsdal County, western Norway, see Figure 4.1. This rockslide is located in an fjord where many historical landslides have been mapped [Blikra et al., 2006]. This area draws considerable attention due to the hazard of a tsunami, generated as a result of a large rock slope failure.

The Åknes rockslide is one of the most investigated and monitored rockslides in the world. The investigations include both regional mapping in the fjord region and a multitude of site specific investigations [Blikra et al., 2008, Ganerød et al., 2008, Kveldsvik et al., 2009, Nordvik and Nyrnes, 2009, Nordvik et al., 2009, Grøneng et al., 2009, Grøneng et al., 2010a, Grøneng et al., 2010b].

At the Åknes site, steep topography and vegetation limit the InSAR coherence between successive SAR acquisitions. In fall of 2005, we installed four radar corner reflectors. SAR data from three parallel Envisat ASAR tracks have been regularly acquired in the period 2005–2010, and RADARSAT-2 Fine and Ultra-fine modes, as well as TerraSAR-X data are currently being acquired. Processing of this data is ongoing [Lauknes et al., 2009].

The Åknes area has been the study location for the work presented in Section 4.3.1 and in Chapter 6.

4.1.2 Nordnes

The *Nordnes* rockslide is located in Lyngen, Troms County, northern Norway, see Figure 4.1. The area of Lyngen is one area in Norway where rockslides cluster [Braathen et al., 2004, Blikra et al., 2006]. This arctic area contains several mapped unstable rockslopes within the periglacial regions with potential permafrost[1]. In northern Norway, permafrost represents a significant feature of the landscape, mainly in mountainous areas. As permafrost contains varying amounts of ground ice, permafrost degradation may affect slope stability. In order to evaluate rockslide geohazards, improved knowledge on the coupling between permafrost and surface slope stability is essential.

Annual GPS measurements, carried out since 2003, and continuous laser and crackmeter measurements from the period October 2007 to April 2009, indicate annual displacement rates between 1–5 cm [Eiken, 2008, Blikra et al., 2009, Nordvik et al., 2010]. The ongoing monitoring system at Nordnes currently includes 3 lasers, 11 crackmeters, 3 extensometers, and a network of 11 continuous GPS monuments, plus 4 satellite radar reflectors.

In the Lyngen area, InSAR is currently being used on an operational basis for regional landslide mapping [Henderson et al., 2007, Henderson et al., 2008, Henderson et al., 2009]. In addition, we have, since autumn of 2008 regularly acquired both ascending and descending high resolution RADARSAT-2 Ultra-fine, and since the start of the 2009 summer season TerraSAR-X SAR data covering the Lyngen area.

The Nordnes rockslide has been the study location for the work presented in Section 4.4 and the regional Lyngen area has been the study area for the work in chapters 7– 9.

[1] Permafrost is defined as subsurface earth materials that remain continuously at or below 0° C for two or more years.

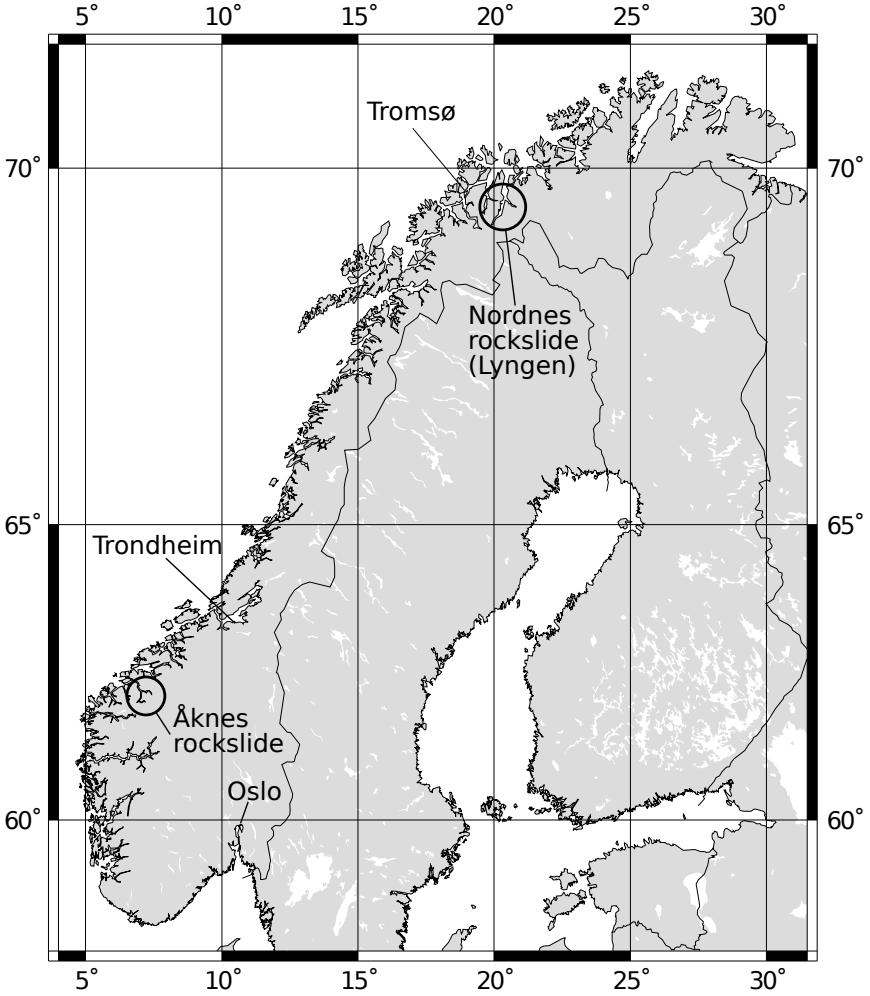

Figure 4.1: The two main rockslide study areas in Norway, Åknes and Nordnes. This map was produced using the Generic Mapping Tools (GMT) [Wessel and Smith, 1998].

4.2 InSAR Processing Challenges in Norway

4.2.1 Irregular data sampling

It is well known that wet snow leads to interferometric decorrelation due to high dielectric losses [Ulaby et al., 1982], while even dry snow will introduce a large phase signal component correlated to the snow water equivalent [Guneriussen et al., 2001]. A challenge when performing InSAR processing in arctic regions is that most parts of the ground are covered by snow during the winter season. Furthermore, the ground at the highest elevations can still be snow covered until mid summer. In effect, we can only include SAR images from approximately June–September in the InSAR processing, leading to an irregular sampling of the SAR data. This has several implications for InSAR time series analysis;

- The irregular sampling, and in particular the long time period between each snow free season with data, affects temporal atmospheric filtering. We can with the 35-day repeat cycle of the ERS and Envisat satellites typically only get 4–5 snow free scenes per year. The data samples are then clustered along the time dimension with a regular time spacing of approximately half a year between clusters. For the temporal atmospheric filtering applied[2], we need to apply long filter lengths that span between two seasons. Such an irregularity in the atmospheric filter length may lead to filter end effects.

- The long temporal separation between some SAR image acquisitions imposes a limit on the maximum surface displacement that can be detected between isolated coherent areas. If the displacement is more than half the wavelength of the radar (see Table 2.1 for a summary of radar properties) between the last image of one year and the first the next year, the displacement signal will be *aliased*, and consequently the total displacement will be underestimated.

- Few SAR scenes each summer limit the analysis to studies of long-term or inter-annual displacement trends. Intraseasonal displacement variations are difficult, if not impossible, to detect. In arctic regions with permafrost, the seasonal thaw-freeze cycle of the active layer causes settlement and uplift of certain landforms, with an amplitude of up to several centimeters [Lauknes et al., 2010].

- Lastly, the fact that we are using snow free scenes only leads to a relatively low number of total images available for time series processing. For a typical area in northern Norway, only 15–20 ERS-1/2 scenes exist in the archive, with on average 3–5 scenes per season. This number is lower than most other reported time series InSAR studies. It should be noted that as sensors with shorter revisit times become available (e.g., RADARSAT-2 with 24 days, TerraSAR-X with 11 days, and ESA Sentinel-1 with 12 days), the potential number of processable scenes per season will significantly increase.

4.2.2 Sparse phase unwrapping

A typical interferogram is often divided into several disconnected coherent areas, separated by large decorrelated areas. In a typical fjord landscape, such as in coastal Norway, this is manifested in the form of interferograms which include large, decorrelated parts with water. The decorrelated water areas can introduce ambiguities for traditional 2D phase unwrapping methods.

In order to exclude the decorrelated areas, the common approach in SBAS methods is to perform a pixel thresholding, selecting only the pixels exhibiting an estimated coherence value larger than a selected threshold in a chosen fraction of the interferograms.

[2]See e.g. [Ferretti et al., 2000, Berardino et al., 2002] for a description of the atmospheric filtering strategy applied in most InSAR time series methods.

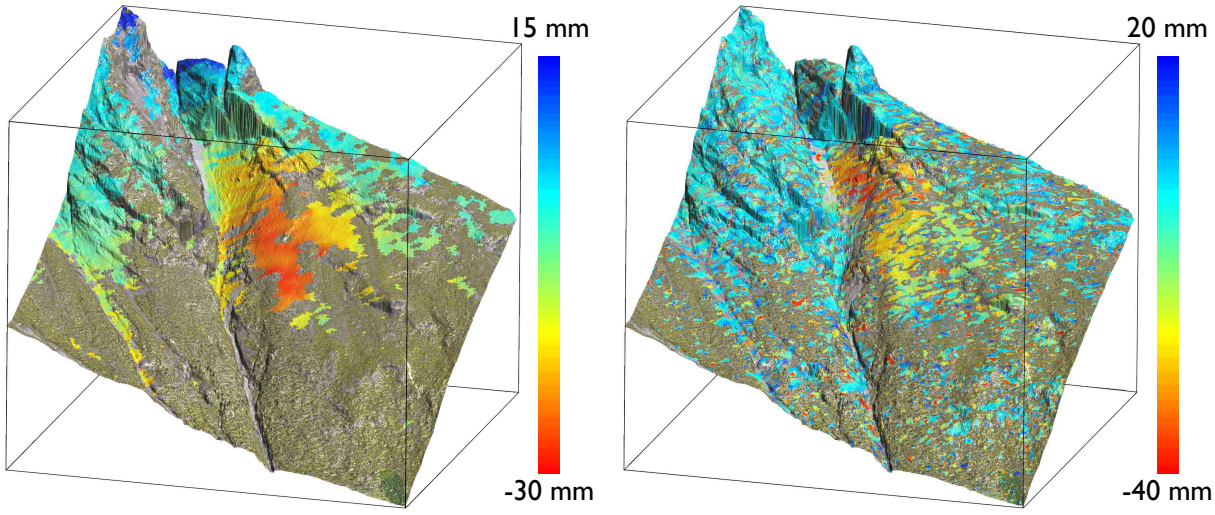

(a) (b)

Figure 4.2: Displacement results (LOS velocity in mm/year) at the Åknes rockslide. Preliminary RADARSAT-2 SBAS results based on Ultra-fine mode data (left), and LISALab results (right) [Lauknes et al., 2009].

By performing this operation, we are able to retain the coherent areas, but we are left with sparse interferograms. The sparse interferograms can then be filled in using a Delaunay triangulation and interpolation [Costantini and Rosen, 1999]. The interpolation allows us to link spatially separated coherent patches. We use linear interpolation between the sparse points. However, nearest neighbor interpolation can also be applied to convert the sparse data set to an equivalent regularly spaced 2D data set [Shanker and Zebker, 2009]. Following this operation, we unwrap all interferograms using the SNAPHU 2D regular grid solver [Chen and Zebker, 2001]. However, we have observed that this approach can produce interferograms with significant unwrapping errors, in particular across the fjords, or across areas with severe layover.

Most unwrapping algorithms unwrap consistently within a coherent area; however, relative values between the different coherent patches may have unknown integer multiples of 2π phase jumps. If one of these jumps is not known accurately, the unwrapped phase field can have large discontinuities. For each selected coherent pixel in the SBAS method, the measured time vector of all unwrapped interferograms will include spikelike noise from each patch that is initially unwrapped with the wrong ambiguity value.

In Chapter 5, we propose an extension to the SBAS method that leads to better robustness with respect to phase unwrapping errors in the interferometric data stack. Our method is based on the original SBAS technique, but improves the robustness in the phase inversion step by replacing the L_2-norm cost function with an L_1-norm based cost function, which is known to be less susceptible to spikelike noise.

4.3 Possibilities With New High-Resolution Sensors

As discussed in Section 3.1, the first generation SAR satellites (ERS-1/2, Envisat, RADARSAT-1, JERS-1, ALOS) have proven well suited for InSAR studies to detect land deformation in many different areas. However, these satellites often fail to provide information in areas with low coherence and high displacement gradients.

The new generation X- and C-band sensors (RADARSAT-2 Ultra-fine mode, TerraSAR-X stripmap and spotlight modes, and COSMO-SkyMed) have higher spatial resolution and shorter revisit times, allowing for detection of deformation at both a finer spatial scale, but also making it possible to detect faster varying deformation phenomena [Prati et al., 2010, Sansosti et al., 2010, Strozzi et al., 2010, Wegmüller et al., 2010]. The high spatial resolution allows for a finer sampling of the deformation phenomena, thereby increasing the potential to discern coherent areas within vegetated regions. The shorter repeat intervals allows detection of larger magnitude displacements between two scenes, reducing the risk of undersampling. In effect, these improvements reduce the complexity of phase unwrapping. Furthermore, TerraSAR-X and COSMO-SkyMed operate at X-band, which gives higher sensitivity than C-band sensors to discern fine scale displacements.

An understanding of the 3D kinematics of the rockslope is essential for hazard analysis [Braathen et al., 2004, Henderson and Saintot, 2009], and it is expected that the new generation SAR sensors can further improve the knowledge of both spatial and temporal rockslide movement patterns. For fast moving landslides, it can be expected that many more objects will be detected. These objects may have been discarded previously due to signal decorrelation, or they have been classified as slow-moving due to temporal undersampling.

4.3.1 Mapping of the Åknes rockslide using RADARSAT-2 Ultra-fine data

Here, we present preliminary results from an ongoing research project where we record high-resolution RADARSAT-2 Ultra-fine mode data over the Åknes rockslide. We have performed a preliminary SBAS InSAR analysis of the Åknes rockslide using only eight RADARSAT-2 Ultra-fine mode SAR scenes [Lauknes et al., 2009]. Figure 4.2(a) shows the mean LOS velocity in mm/year for the rockslide area. The SAR data have been multilooked to produce pixels with ground sizes of approximately 10 m, and the results have been draped on a high resolution DEM.

In order to better understand the complex movement pattern at Åknes, the LISALab ground based interferometric SAR (GB-InSAR) system was installed and operated between July 17 and October 13, 2008. Figure 4.2(b) shows the mean LOS velocity in mm/year.

The preliminary results using the RADARSAT-2 Ultra-fine mode data show a good match with the LISALab GB-InSAR results. It should be noted that the radar LOS direc-

tions are quite different, so an exact comparison is yet to be done. More RADARSAT-2 Ultra-fine scenes are continuously being added to this time series.

4.4 Monitoring of the Nordnes Rockslide Using Radar Corner Reflectors

Not all known landslides have sufficient InSAR coherence, due to steep topography and vegetation, leading to few or no coherent points. Another consideration is that after a rockslide has been classified as a risk object, the government is interested in a year-round monitoring of the active slopes. In these cases, it is possible to install radar corner reflectors. The radar reflectors act as discrete targets, that permit regular monitoring by use of a simplified PSI InSAR technique [Ferretti et al., 2007]. The reflectors are covered to prevent snow accumulation, thus allowing regular acquisition of SAR data throughout the year. By using radar corner reflectors, it is possible to move from from mapping to regular *monitoring* of selected objects.

Here, we present preliminary results from the ongoing reflector experiment at Nordnes [Lauknes and Larsen, 2010]. Parts of the unstable area at the Nordnes landslide, which lies at an altitude of about 600–800 meters above sea level, are moving with a rate of up to 5–6 cm per year [Eiken, 2008,Henderson et al., 2009]. Previous InSAR studies in this area have been unsuccessful in observing these high rates, probably due to signal aliasing.

4.4.1 Corner reflectors

At the Nordnes rockslide, four 1.8 m trihedral radar corner reflectors were deployed in October 2009, see Figure 4.3. The reflectors are covered with a custom made PVC plastic to keep snow from accumulating in the reflector, while being transparent to the electromagnetic waves. The reflectors were installed at four selected locations (*refl0*–*refl3*), with one reference site (*refl0*) assumed stable, see Table 4.1.

4.4.2 Satellite data

The main satellite sensor for continuous long-term monitoring of Nordnes is RADARSAT-2 Fine Mode.

Here, we report results from InSAR analysis of 13 RADARSAT-2 Fine Mode scenes acquired in the period from 24 November 2009 to 13 December 2010, 6 RADARSAT-2 Ultra-fine mode scenes acquired in the period 21 May 2010 to 12 October 2010, 7 Envisat ASAR scenes from track 22 acquired in the period 4 November 2009 to 15 September 2010, 8 Envisat ASAR scenes from track 251 acquired in the period 20 November 2009 to 1 October 2010, and 9 TerraSAR-X Stripmap mode scenes acquired in the period 22 November 2009 to 15 September 2010.

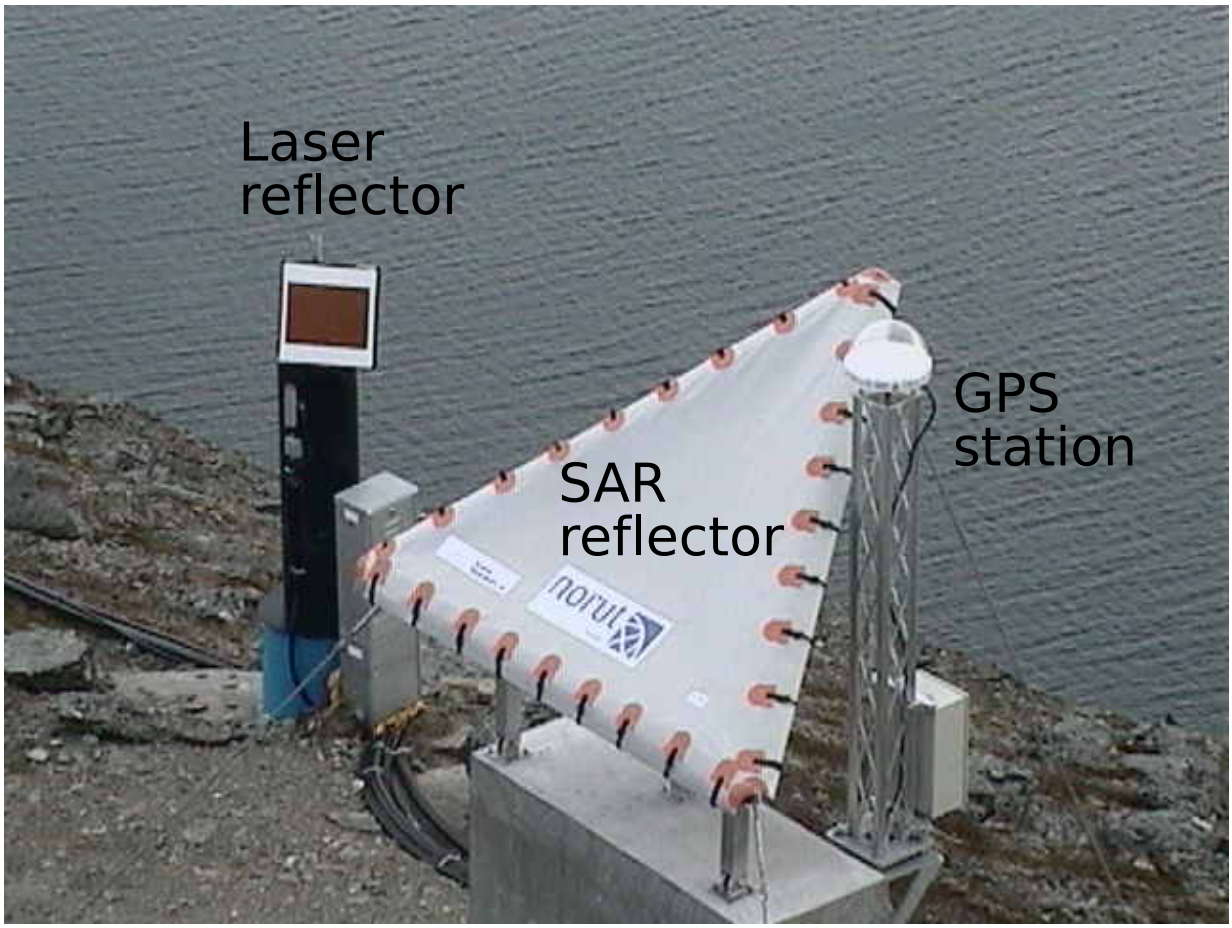

Figure 4.3: Location of *refl1* at the Nordnes rockslide. The reflector is mounted on a concrete pillar, and is collocated with the YN3 GPS station and a laser reflector.

All data are acquired in *descending mode*.

4.4.3 InSAR processing of the reflector double differences

For each of the satellite sensors used, a simplified PSI processing similar to [Ferretti et al., 2001, Lauknes and Larsen, 2007] was used to estimate the double-difference displacement rates. Precise height information from collocated GPS receivers were used to remove the topographic phase contribution.

Displacement time series were estimated for all satellite tracks, between all reflector combinations. The vertical component was estimated by multiplication with $\cos\theta$, where θ is the incidence angle.

4.4.4 Displacement results

Figure 4.4 shows the displacement time series between reflector 1 (*refl1*) and reflector 0 (*refl0*), assumed located on stable ground. The collocated GPS vertical time series is shown in Figure 4.4(b).

We were unable to provide a reliable estimate of the displacement of reflector 3 (*refl3*). This reflector is located at approximately 400–500 m lower altitude than the other reflectors. Consequently, the double differences between this reflector and the ones higher up introduce an atmospheric phase component related to the atmospheric stratification. Further work will use the GPS data to estimate and mitigate the atmospheric phase/delay in the InSAR measurements, as described in Chapter 6.

4.4.5 Corner reflector summary

The reflectors perform according to expectations. The mechanical design is able to withstand the harsh weather conditions at the Nordnes site, and the plastic snow cover is able to keep snow from accumulating in the reflectors. However, under certain meteorological conditions, the plastic cover can accumulate a thin snow layer, which can introduce a phase delay. This can partly explain the small scale (a few mm) variations observed in the displacement time series. In our experience, the plastic cover is sufficient to protect the reflectors. Vibrations in the plastic cover due to blowing wind is often sufficient to remove this layer.

The displacement results between the three upper reflectors (*refl0–refl2*) show that we are able to produce robust results using as few as 6 scenes (Envisat ASAR track 22), as long as the temporal spacing is sufficiently dense to avoid signal aliasing. The total deformation between the upper three reflector pairs add up to zero around a closed loop, indicating a robust and correct displacement estimation.

The results illustrate that the long-term monitoring data (based on RADARSAT-2 with 24 days repeat cycle) can be filled in with other data with higher temporal resolution (e.g. TerraSAR-X with 11 days repeat cycle) in periods where such data is available.

Table 4.1: Location of corner reflectors, Nordnes site.

Station Id.	Latitude (degrees)	Longitude (degrees)	Altitude (m)
refl0	69.557955	20.417210	753.5
refl1	69.557253	20.411969	688.8
refl2	69.555699	20.409442	652.6
refl3	69.558842	20.397328	250.6

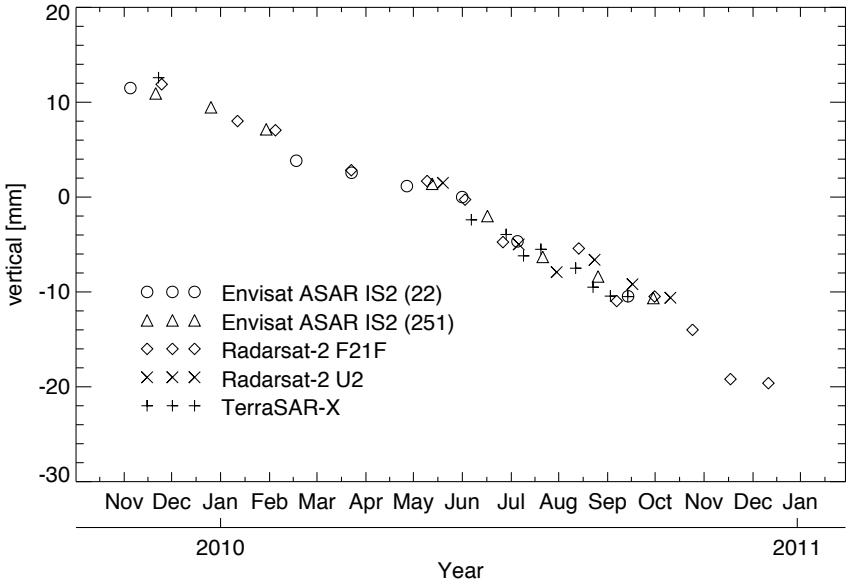

(a)

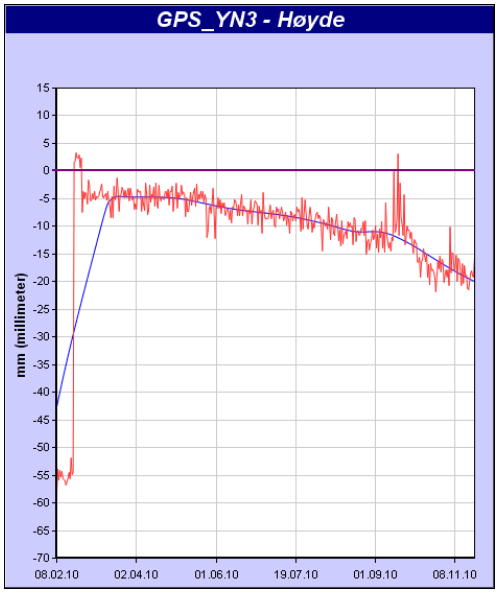

(b)

Figure 4.4: (a) Displacement time series for *refl1* relative to the reference reflector for different SAR sensors. (b) Vertical displacement estimated from GPS station YN3, which is collocated with *refl1*. Source: Fjellskred i Troms.

Chapter 5

Paper 1:
InSAR Deformation Time Series Using an L_1-norm Small-Baseline Approach

Chapter 6

Paper 2:
InSAR Tropospheric Stratification Delays: Correction Using a Small Baseline Approach

Chapter 7

Paper 3:
Detailed rockslide mapping in northern Norway with small baseline and persistent scatterer interferometric SAR time series methods

Chapter 8

Paper 4:
A structural, geomorphological and InSAR study of an active rock slope failure development

Chapter 9

Paper 5:
Active normal fault control on landscape and rock-slope failure in northern Norway

Chapter 10

Conclusions

In this chapter, we give concluding remarks and suggestions for future research.

10.1 Summary

The research topic of this study has been development and application of SB InSAR time series methods for extracting information about ground surface stability in rural terrain, with a main focus on rockslides. The work has concentrated on improvements to the well known SBAS method, to make detecting surface displacements in arctic terrain feasible.

In chapters 2–3 of this thesis, we presented a brief background on the principles behind SAR imaging and an introduction to the InSAR concept. The chapters were written with a nonspecialist in mind, focusing on the limitations and strengths of the InSAR satellite remote sensing tool.

Chapter 4 contains a discussion on the particular InSAR challenges we faced in the study areas in Norway, mainly focusing on the steep topography and high relief causing unwrapping problems and prominent atmospheric stratification effects, as well as the challenge with long periods with snow. We concluded Chapter 4 by presenting possibilities with new satellite sensors, and we presented two preliminary results from ongoing InSAR mapping and monitoring projects in Norway. The first considers *mapping* of the Åknes landslide with high-resolution RADARSAT-2 data, and the second one considers year round *monitoring* of the Nordnes landslide using radar corner reflectors.

Chapters 5–9 include the 5 papers that make up the core of the thesis. The first two papers contribute to new technology insight, while the last three present applications where the technology has been used.

The research has demonstrated that time series InSAR is a powerful tool which can be used to identify the relative magnitude and spatial pattern of rockslides. On the *regional* scale, large areas can be determined to be stable, thereby allowing rather expensive field activities to be focused on areas where movement has been detected. On the *local* scale, the InSAR data have contributed to the detailed interpretation of the failure

mechanism of several rockslides. Our extensive experience in the ground-truthing of the InSAR method demonstrates a remarkable correlation between subsidence detected from the InSAR and mappable, unstable slopes in the terrain.

We have demonstrated that the time series InSAR methodology provides a new and unprecedented technique to determine potential rockslide movement and therefore provides a direct link between quantitative ground movement data and the structures, kinematics and changes of slope.

We conclude that time series InSAR is a valuable tool in providing quantitative data of the activity in rockslides. For year round *monitoring* of high-risk objects in arctic regions, radar corner reflectors must be installed.

10.2 Suggestions for Further Work

Robust 2D or 3D phase unwrapping is crucial for successful application of small baseline InSAR methods. Future work should focus on development of faster and more reliable unwrapping algorithms that are optimized for sparsely coherent datasets.

The exploitation of partially coherent targets, plus development of InSAR methods that utilize information from both persistent point targets as well as from areas with distributed scattering, is expected to increase the spatial density of points, in particular in rural areas [Hooper et al., 2004, Lanari et al., 2004, Perissin et al., 2007, Prati et al., 2010].

For the Åknes radar corner reflector project, future work will apply atmospheric path delay information inferred from the GPS network, to correct for the path delay correlating with topography. Such correction is imperative in order to robustly estimate displacement of radar corner reflectors in steep terrain.

In Norway, permafrost represents a significant feature of the landscape, mainly in mountainous areas, and it is well known that thawing permafrost can have a substantial impact of slope stability. In order to evaluate the rockslide geohazard, improved knowledge on the relationship between ground stability and thawing permafrost is essential.

The new satellite sensors, with increased spatial resolution and shorter revisit times, will hopefully permit us to use advanced InSAR time series methods to better quantify and understand the *temporal* deformation patterns of different landscape forms in areas with permafrost. However, much work still remains for proper understanding of the interaction between the measured InSAR displacement signal and the variety of spatial and temporal surface movements recorded in the different permafrost landforms.

Bibliography

[Amelung et al., 2000] F. Amelung, S. Jónsson, H. Zebker and P. Segall. *Widespread uplift and 'trapdoor' faulting on Galápagos volcanoes observed with radar interferometry*. *Nature*, **407**: 993–996, 2000. doi:10.1038/35039604.

[Bamler and Hartl, 1998] R. Bamler and P. Hartl. *Synthetic aperture radar interferometry*. *Inverse Problems*, **14**: R1–R54, 1998. doi:10.1088/0266-5611/14/4/001.

[Beauducel et al., 2000] F. Beauducel, P. Briole and J.-L. Froger. *Volcano-wide fringes in ERS synthetic aperture radar interferograms of Etna (1992-1998): Deformation or tropospheric effect?*. *J. Geophys. Res.*, **105**(B7): 391–402, 2000.

[Berardino et al., 2002] P. Berardino, G. Fornaro, R. Lanari and E. Sansosti. *A new algorithm for surface deformation monitoring based on small baseline differential SAR interferograms*. *IEEE Transactions on Geoscience and Remote Sensing*, **40**(11): 2375–2383, Nov. 2002. doi:10.1109/TGRS.2002.803792.

[Berardino et al., 2003] P. Berardino, M. Costantini, G. Franceschetti, A. Iodice, L. Pietranera and V. Rizzo. *Use of differential SAR interferometry in monitoring and modelling large slope instability at Maratea (Basilicata, Italy)*. *Engineering Geology*, **68**: 31–51, 2003. doi:10.1016/S0013-7952(02)00197-7.

[Blikra et al., 2006] L. H. Blikra, O. Longva, A. Braathen, E. Anda, J. Dehls and K. Stalsberg. *Rock-slope failures in Norwegian fjord areas: examples, spatial distribution and temporal pattern*. In *Landslides from Massive Rock Slope Failure: NATO Science Series: IV: Earth and Environmental Sciences*, volume 49. 2006.

[Blikra et al., 2008] L. H. Blikra, K. Jogerud, J. Hole and T. Bergeng. *The Åknes/Tafjord project – Monitoring and implementation of early-warning systems*. In *European Geosciences Union Program with Abstracts, General Assembly 2008, Vienna, 13–18 April 2008: Geophysical Research Abstracts*. 2008.

[Blikra et al., 2009] L. H. Blikra, I. Henderson and T. Nordvik. *Faren for fjellskred fra Nordnesfjellet i Lyngenfjorden, Troms*. Report 2009.026, Geological Survey of Norway, 2009. (in Norwegian).

[Bonforte et al., 2001] A. Bonforte, A. Ferretti, C. Prati, G. Puglisi and F. Rocca. *Calibration of atmospheric effects on SAR interferograms by GPS and local atmosphere models: first results*. *Journal of Atmospheric and Solar-Terrestrial Physics*, **63**(12): 1343–1357, 2001. doi:10.1016/S1364-6826(00)00252-2.

[Braathen et al., 2004] A. Braathen, L. H. Blikra, S. S. Berg and F. Karlsen. *Rock-slope failures in Norway; type, geometry, deformation mechanisms and stability*. *Norwegian Journal of Geology*, **84**: 67–88, 2004.

[Cavalié et al., 2007] O. Cavalié, M.-P. Doin, C. Lasserre and P. Briole. *Ground motion measurement in the Lake Mead area, Nevada, by differential synthetic aperture radar interferometry time series analysis: Probing the lithosphere rheological structure*. *Journal of Geophysical Research*, **112**(B03403), 2007. doi:10.1029/2006JB004344.

[Chaabane et al., 2007] F. Chaabane, A. Avallone, F. Tupin, P. Briole and H. Mâitre. *A multitemporal method for correction of tropospheric effects in differential SAR interferometry: Application to the Gulf of Corinth earthquake*. *IEEE Transactions on Geoscience and Remote Sensing*, **45**(6), 2007. doi:10.1109/TGRS.2007.894026.

[Chen and Zebker, 2000] C. W. Chen and H. A. Zebker. *Network approaches to two-dimensional phase unwrapping: intractability and two new algorithms*. *Journal of the Optical Society of America A.*, **17**(3): 401–414, 2000. doi:10.1364/JOSAA.17.000401.

[Chen and Zebker, 2001] C. W. Chen and H. A. Zebker. *Two-dimensional phase unwrapping with use of stastistical models for cost functions in nonlinear optimization*. *Journal of the Optical Society of America A.*, **18**(2): 338–351, 2001. doi:10.1364/JOSAA.18.000338.

[Colesanti and Wasowski, 2006] C. Colesanti and J. Wasowski. *Investigating landslides with space-borne Synthetic Aperture Radar (SAR) interferometry*. *Engineering Geology*, **88**(3–4): 173–199, 2006. doi:10.1016/j.enggeo.2006.09.013.

[Costantini, 1998] M. Costantini. *A novel phase unwrapping method based on network programming*. *IEEE Transactions on Geoscience and Remote Sensing*, **36**(3): 813–821, May. 1998. doi:10.1109/36.673674.

[Costantini and Rosen, 1999] M. Costantini and P. A. Rosen. *A generalized phase unwrapping approach for sparse data*. *Proc. IGARSS, Hamburg, Germany, Jun. 28–Jul. 2*, **1**: 267–269, 1999. doi:10.1109/IGARSS.1999.773467.

[Cumming and Wong, 2005] I. G. Cumming and F. H. Wong. *Digital Processing of Synthetic Aperture Radar Data: Algorithms and Implementation*. Artech House Inc., New York, 2005.

[Curlander and McDonough, 1991] J. C. Curlander and R. N. McDonough. *Synthetic Aperture Radar*. Wiley, 1991.

[Davis et al., 1985] J. L. Davis, T. A. Herring, I. I. Shapiro, A. E. E. Rogers and G. Elgered. *Geodesy by radio interferometry: Effects of atmospheric modeling errors on estimates of baseline length*. *Radio Science*, **20**(6): 1593–1607, 1985.

[Dehls et al., 2002] J. F. Dehls, M. Basilico and C. Colesanti. *Ground deformation monitoring in the Ranafjord area of Norway by means of the permanent scatterers technique*. *Proc. IGARSS, Toronto, Canada, June 24–28*, **1**: 203–207, 2002. doi:10.1109/IGARSS.2002.1024988.

[Delacourt et al., 1998] C. Delacourt, P. Briole and J. A. Achache. *Tropospheric corrections of SAR interferograms with strong topography. Application to Etna*. *Geophysical Research Letters*, **25**(15): 2849–2852, 1998. doi:10.1029/98GL02112.

[Doin et al., 2009] M.-P. Doin, C. Lasserre, G. Peltzer, O. Cavalié and C. Doubre. *Corrections of stratified tropospheric delays in SAR interferometry: Validation with global atmospheric models*. *Journal of Applied Geophysics*, **69**(1): 35–50, 2009. doi:10.1016/j.jappgeo.2009.03.010.

[Eiken, 2008] T. Eiken. *Rapport om Deformasjonsmålingar i Troms 2003–2008*. Technical report, University of Oslo, 2008. (in Norwegian).

[Ferretti et al., 2000] A. Ferretti, C. Prati and F. Rocca. *Nonlinear subsidence rate estimation using permanent scatterers in differential SAR interferometry*. *IEEE Transactions on Geoscience and Remote Sensing*, **38**(5): 2202–2212, Sep. 2000. doi:10.1109/36.868878.

[Ferretti et al., 2001] A. Ferretti, C. Prati and F. Rocca. *Permanent scatterers in SAR interferometry*. *IEEE Transactions on Geoscience and Remote Sensing*, **39**(1): 8–20, Jan. 2001. doi:10.1109/36.898661.

[Ferretti et al., 2007] A. Ferretti, G. Savio, R. Barzaghi, A. Borghi, S. Musazzi, F. Novali, C. Prati and F. Rocca. *Submillimeter accuracy of InSAR time series: experimental validation*. *IEEE Transactions on Geoscience and Remote Sensing*, **45**(5): 1142–1153, 2007. doi:10.1109/TGRS.2007.894440.

[Franceschetti and Lanari, 1999] G. Franceschetti and R. Lanari. *Synthetic Aperture Radar Processing*. CRC Press, 1999.

[Gabriel et al., 1989] A. K. Gabriel, R. M. Goldstein and H. A. Zebker. *Mapping small elevation changes over large areas: Differential radar interferometry*. *Journal of Geophysical Research*, **94**(B7): 9183–9191, 1989. Doi:10.1029/JB094iB07p09183.

[Ganerød et al., 2008] G. V. Ganerød, G. Grøneng, J. S. Rønning, E. Dalsegg, H. Elvebakk, J. F. Tønnesen, V. Kveldsvik, T. Eiken, L. H. Blikra and A. Braathen. *Geological model of the Åknes rockslide, western Norway*. *Engineering Geology*, **102**(1–2): 1–18, 2008. doi:10.1016/j.enggeo.2008.01.018.

[Gatelli et al., 1994] F. Gatelli, A. M. Guarnieri, F. Parizzi, P. Pasquali, C. Prati and F. Rocca. *The wavenumber shift in SAR interferometry*. *IEEE Transactions on Geoscience and Remote Sensing*, **32**(4): 855–865, 1994. doi:10.1109/36.298013.

[Ghiglia and Pritt, 1998] D. C. Ghiglia and M. D. Pritt. *Two-dimensional Phase Unwrapping: Theory, Algorithms, and Software,*. Wiley, New York, 1998.

[Goldstein, 1995] R. M. Goldstein. *Atmospheric limitations to repeat-track radar interferometry*. *Geophysical Research Letters*, **22**(18): 2517–2520, 1995. doi:10.1029/95GL02475.

[Goldstein et al., 1988] R. M. Goldstein, H. A. Zebker and C. L. Werner. *Satellite radar interferometry: Two-dimensional phase unwrapping*. *Radio Science*, **23**(4): 713–720, 1988. doi:10.1029/RS023i004p00713.

[Goldstein et al., 1993] R. M. Goldstein, R. Engelhardt, B. Kamp and R. M. Frolich. *Satellite radar interferometry for monitoring ice sheet motion: Application to an Antarctic ice stream*. *Science*, **262**: 1525–1530, 1993. doi:10.1126/science.262.5139.1525.

[Graham, 1974] L. C. Graham. *Synthetic Interferometer Radar for Topographic Mapping*. *Proceedings of the IEEE*, **62**(6): 763–768, 1974. doi:10.1109/PROC.1974.9516.

[Grøneng et al., 2009] G. Grøneng, B. Nilsen and R. Sandven. *Shear strength estimation for Åknes sliding area in western Norway*. *International Journal of Rock Mechanics & Mining Sciences*, **46**(3): 479–488, 2009. doi:10.1016/j.ijrmms.2008.10.006.

[Grøneng et al., 2010a] G. Grøneng, H. H. Christiansen, B. Nilsen and L. H. Blikra. *Meteorological effects on seasonal displacements of the Åknes rockslide, western Norway*. *Landslides*, 2010a. doi:10.1007/s10346-010-0224-x.

[Grøneng et al., 2010b] G. Grøneng, M. Lu, B. Nilsen and A. K. Jenssen. *Modelling of time-dependent behavior of the basal sliding surface of the Åknes rockslide area in western Norway*. *Engineering Geology*, **114**(3–4): 414–422, 2010b. 10.1016/j.enggeo.2010.05.017.

[Guneriussen et al., 2001] T. Guneriussen, K. A. Høgda, H. Johnsen and I. Lauknes. *InSAR for estimation of changes in snow water equivalent of dry snow*. *IEEE Transactions on Geoscience and Remote Sensing*, **39**(10): 2101–2108, 2001. doi:10.1109/36.957273.

[Hanssen, 2001] R. Hanssen. *Radar Interferometry: Data Interpretation and Error Analysis*. Kluwer Academic, Dordrecht, The Netherlands, 2001.

[Hanssen and Usai, 1997] R. Hanssen and S. Usai. *Interferometric phase analysis for monitoring slow deformation processes*. In *Proc. Third ERS Symp., Florence, Italy, Mar. 17–21*, pp. 487–491. 1997.

[Henderson and Saintot, 2009] I. H. C. Henderson and A. Saintot. *Regional spatial variations in rockslide distribution from structural geology ranking: an example from Storfjorden, western Norway*. *Slope Tectonics, Geological Society, London, Special Publications*, 2009. (in press).

[Henderson et al., 2007] I. H. C. Henderson, A. Saintot, G. V.-G. d and L. H. Blikra. *Fjellskredkartlegging i Troms*. Report 2007.041, Geological Survey of Norway, 2007. (in Norwegian).

[Henderson et al., 2008] I. H. C. Henderson, P. T. Osmundsen and T. F. Redfield. *ROS Fjellskred i Troms: Statusrapport*. Report 2008.025, Geological Survey of Norway, 2008. (in Norwegian).

[Henderson et al., 2009] I. H. C. Henderson, P. T. Osmundsen and T. F. Redfield. *ROS Fjellskred i Troms: Status og planer*. Report 2009.023, Geological Survey of Norway, 2009. (in Norwegian).

[Hilley et al., 2004] G. E. Hilley, R. Bürgmann, A. Ferretti, F. Novali and F. Rocca. *Dynamics of slow-moving landslides from permanent scatterer analysis*. *Science*, **304**(5679): 1952–1955, 2004. doi:10.1126/science.1098821.

[Hooper, 2008] A. Hooper. *A multi-temporal InSAR method incorporating both persistent scatterer and small baseline approaches*. *Geophysical Research Letters*, **35**(L16302), 2008. doi:10.1029/2008GL034654.

[Hooper and Zebker, 2007] A. Hooper and H. A. Zebker. *Phase unwrapping in three dimensions with application to InSAR time series*. *Journal of the Optical Society of America A.*, **24**(9): 2737–2747, 2007. doi:10.1364/JOSAA.24.002737.

[Hooper et al., 2004] A. Hooper, H. Zebker, P. Segall and B. Kampes. *A new method for measuring deformation on volcanoes and other natural terrains using InSAR persistent scatterers*. *Geophysical Research Letters*, **31**(L23611), 2004. doi:10.1029/2004GL021737.

[Hooper et al., 2007] A. Hooper, P. Segall and H. Zebker. *Persistent scatterer interferometric synthetic aperture radar for crustal deformation analysis, with application to Volcán Alcedo, Galápagos*. *Journal of Geophysical Research*, **112**(B07407), 2007. doi:10.1029/2006JB004763.

[Ishimaru, 1978] A. Ishimaru. *Wave Propagation and Scattering in Random Media*. Academic Press, 1978.

[Kampes, 2006] B. M. Kampes. *Radar Interferometry - Persistent Scatterer Technique*. Springer, Dordrecht, The Netherlands, 2006.

[Kveldsvik et al., 2009] V. Kveldsvik, H. H. Einstein, B. Nilsen and L. H. Blikra. *Numerical analysis of the 650,000 m^2 Åknes rock slope based on measured displacements*

and geotechnical data. *Rock Mechanics and Rock Engineering*, **42**(5): 689–728, 2009. doi:10.1007/s00603-008-0005-1.

[Lanari et al., 2004] R. Lanari, O. Mora, M. Manuta, J. J. Mallorquí, P. Berardino and E. Sansosti. *A small-baseline approach for investigating deformations on full-resolution differential SAR interferograms*. *IEEE Transactions on Geoscience and Remote Sensing*, **42**(7): 1377–1386, 2004. doi:10.1109/TGRS.2004.828196.

[Lanari et al., 2007] R. Lanari, F. Casu, M. Manzo, G. Zeni, P. Berardino, M. Manuta and A. Pepe. *An overview of the small baseline subset algorithm: A DInSAR technique for surface deformation analysis*. *Pure and Applied Geophysics*, **164**(4): 637–661, Apr. 2007. doi:10.1007/s00024-007-0192-9.

[Lauknes, 2004] T. R. Lauknes. *Long-Term Surface Deformation Mapping using Small-Baseline Differential SAR Interferograms*. Master's thesis, University of Tromsø, Norway, 2004.

[Lauknes and Larsen, 2007] T. R. Lauknes and Y. Larsen. *Persistent scatterer interferometric SAR*. Report 2007.15, Norut Tromsø, 2007.

[Lauknes and Larsen, 2010] T. R. Lauknes and Y. Larsen. *Nordnes InSAR corner reflector status report 2010*. Report 2010.18, Norut Tromsø, 2010.

[Lauknes et al., 2009] T. R. Lauknes, J. F. Dehls, Y. Larsen and L. H. Blikra. *Monitoring of the Åknes rockslide in Storfjorden, Norway using InSAR*. In *Abstract. Fringe 2009 Workshop, ESA ESRIN, Frascati, Rome, Nov. 30–Dec. 4*. 2009.

[Lauknes et al., 2010] T. R. Lauknes, Y. Larsen, E. Malnes and H. H. Christiansen. *Permafrost monitoring using SAR and ground based techniques in Svalbard*. In *Abstract, Third European Conference on Permafrost (EUCOP III), Longyearbyen, Svalbard, Norway, June 13–17*. 2010.

[Lohman and Simons, 2005] R. B. Lohman and M. Simons. *Some thoughts on the use of InSAR data to constrain models of surface deformation: Noise structure and data downsampling*. *Geochemistry Geophysics Geosystems*, **6**(Q01007), 2005. doi:10.1029/2004GC000841.

[Lundgren et al., 2001] P. Lundgren, S. Usai, E. Sansosti, R. Lanari, M. Tesauro, G. Fornaro and P. Berardino. *Modelling surface deformation observed with synthetic aperture radar interferometry at Campi Flegrei caldera*. *Journal of Geophysical Research*, **106**(B9): 19355–19366, 2001. doi:10.1029/2001JB000194.

[Massonnet and Feigl, 1998] D. Massonnet and K. L. Feigl. *Radar interferometry and its application to changes in the earth's surface*. *Reviews of Geophysics*, **36**(4): 441–500, 1998. doi:10.1029/97RG03139.

[Massonnet et al., 1993] D. Massonnet, M. Rossi, C. Carmona, F. Adagna, G. Peltzer, K. Feigl and T. Rabaute. *The displacement field of the Landers earthquake mapped by radar interferometry*. *Nature*, **364**(8): 138–142, 1993. doi:10.1038/364138a0.

[Massonnet et al., 1995] D. Massonnet, P. Briole and A. Arnaud. *Deflation of Mount Etna monitored by spaceborne radar interferometry*. *Nature*, **375**: 567–570, 1995. doi:10.1038/375567a0.

[Mora et al., 2003] O. Mora, J. J. Mallorquí and A. Broquetas. *Linear and non-linear terrain deformation maps from a reduced set of interferometric sar images*. *IEEE Transactions on Geoscience and Remote Sensing*, **41**(10): 2243–2253, 2003. doi:10.1109/TGRS.2003.814657.

[Nordvik and Nyrnes, 2009] T. Nordvik and E. Nyrnes. *Statistical analysis of surface displacements-an example from the Aknes rockslide, western Norway*. *Natural Hazards and Earth System Sciences*, **9**: 713–724, 2009. doi:10.5194/nhess-9-713-2009.

[Nordvik et al., 2009] T. Nordvik, G. Grøneng, G. V. Ganerød, B. Nilsen, C. Harding and L. H. Blikra. *Geovisualization, geometric modelling and volume estimation of the Åknes rockslide, Western Norway*. *Bulletin of Engineering Geology and the Environment*, **68**(2): 245–256, 2009. doi:10.1007/s10064-009-0198-x.

[Nordvik et al., 2010] T. Nordvik, L. H. Blikra, E. Nyrnes and M.-H. Derron. *Statistical analysis of seasonal displacements at the Nordnes rockslide, northern Norway*. *Engineering Geology*, **114**(3–4): 228–337, 2010. doi:10.1016/j.enggeo.2010.04.019.

[Peltzer et al., 2001] G. Peltzer, F. Crampé, S. Hensley and P. Rosen. *Transient strain accumulation and fault interaction in the Eastern California shear zone*. *Geology*, **29**(11): 975–978, 2001. doi:10.1130/0091-7613(2001)029.

[Pepe and Lanari, 2006] A. Pepe and R. Lanari. *On the extension of the minimum cost flow algorithm for phase unwrapping of multitemporal differential SAR interferograms*. *IEEE Transactions on Geoscience and Remote Sensing*, **44**(9): 2374–2383, Sep. 2006. doi:10.1109/TGRS.2006.873207.

[Perissin et al., 2007] D. Perissin, A. Ferretti, R. Piantanida, D. Piccagli, C. Prati, F. Rocca, A. Rucci and F. de Zan. *Repeat-pass SAR interferometry with partially coherent targets*. *Proc. Fifth International Workshop on ERS SAR Interferometry, "FRINGE07", ESA ESRIN, Frascati, Rome, November 26–30*, 2007.

[Prati et al., 2010] C. Prati, A. Ferretti and C. Perissin. *Recent advances on surface ground deformation measurement by means of repeated space-borne SAR observations*. *Journal of Geodynamics*, **49**(3–4): 161–170, 2010. doi:10.1016/j.jog.2009.10.011.

[Remy et al., 2003] D. Remy, S. Bonvalot, P. Briole and M. Murakami. *Accurate measurements of tropospheric effects in volcanic areas from SAR interferometry data: application*

to Sakurajima volcano (Japan). *Earth and Planetary Science Letters*, **213**: 299–310, 2003. doi:10.1016/S0012-821X(03)00331-5.

[Rocca et al., 2000] F. Rocca, C. Prati, A. M. Guarnieri and A. Ferretti. *SAR interferometry and its applications*. *Surveys in Geophysics*, **21**(2–3): 159–176, 2000. doi:10.1023/A:1006710731155.

[Rosen et al., 2000] P. A. Rosen, S. Hensley, I. R. Joughin, F. K. Li, S. N. Madsen, E. Rodríguez and R. M. Goldstein. *Synthetic aperture radar interferometry*. *Proceedings of the IEEE*, **88**(3): 333–382, 2000. doi:10.1109/5.838084.

[Rott and Nagler, 2006] H. Rott and T. Nagler. *The contribution of radar interferometry to the assessment of landslide hazards*. *Advances in Space Research*, **37**(4): 710–719, 2006. doi:10.1016/j.asr.2005.06.059.

[Sandwell and Price, 1998] D. T. Sandwell and E. J. Price. *Phase gradient approach to stacking interferograms*. *Journal of Geophysical Research*, **103**(B12): 30183–30204, 1998. doi:10.1029/1998JB900008.

[Sansosti et al., 2010] E. Sansosti, F. Casu, M. Manzu and R. Lanari. *Space-borne radar interferometry techniques for the generation of deformation time series: An advanced tool for Earth's surface displacement analysis*. *Geophysical Research Letters*, **37**(L20305), 2010. doi:10.1029/2010GL044379.

[Schmidt and Bürgmann, 2003] D. A. Schmidt and R. Bürgmann. *Time-dependent land uplift and subsidence in the Santa Clara valley, California, from a large InSAR data set*. *Journal of Geophysical Research*, **108**(B9), 2003. doi:10.1029/2002JB002267.

[Shanker and Zebker, 2009] A. P. Shanker and H. Zebker. *Sparse two-dimensional phase unwrapping using regular grid methods*. *IEEE Geoscience and Remote Sensing Letters*, **6**(3), 2009. doi:10.1109/LGRS.2009.2020522.

[Shanker and Zebker, 2010] A. P. Shanker and H. Zebker. *Edgelist phase unwrapping algorithm for time series InSAR analysis*. *Journal of the Optical Society of America A.*, **27**(3): 605–612, 2010. doi:10.1364/JOSAA.27.000605.

[Strozzi et al., 2000] T. Strozzi, P. Dammert, U. Wegmüller, J. M. Martinez, J. Askne, A. Beaudoin and M. Hallikainen. *Landuse mapping with ERS SAR Interferometry*. *IEEE Transactions on Geoscience and Remote Sensing*, **38**(2): 766–775, 2000. doi:10.1109/36.842005.

[Strozzi et al., 2003] T. Strozzi, U. Wegmüller, C. L. Werner, A. Wiesmann and V. Spreckels. *JERS SAR interferometry for land subsidence monitoring*. *IEEE Transactions on Geoscience and Remote Sensing*, **41**(7): 1702–1708, 2003. doi:10.1109/TGRS.2003.813273.

[Strozzi et al., 2005] T. Strozzi, P. Farina, A. Corsini, C. Ambrosi, M. Thüring, J. Zilger, A. Wiesmann, U. Wegmüller and C. Werner. *Survey and monitoring of landslide displacements by means of L-band satellite SAR interferometry*. *Landslides*, **2**(3): 193–201, 2005. doi:10.1007/s10346-005-0003-2.

[Strozzi et al., 2010] T. Strozzi, R. Delaloye, A. Kääb, C. Ambrosi, E. Perruchoud and U. Wegmüller. *Combined observations of rock mass movements using satellite SAR interferometry, differential GPS, airborne digital photogrammetry, and airborne photography interpretation*. *Journal of Geophysical Research*, **115**(F01014), 2010. doi:10.1029/2009JF001311.

[Ulaby et al., 1982] F. T. Ulaby, R. K. Moore and A. K. Fung. *Microwave Remote Sensing*, volume II. Addison-Wesley, 1982.

[Usai, 1997] S. Usai. *The use of man-made features for long-time scale INSAR*. In *Proc. IGARSS, Singapore, August 3–8*, pp. 1542–1544. 1997.

[Wadge et al., 2002] G. Wadge, P. W. Webley, I. N. James, R. Bingley, A. Dodson, S. Waugh, T. Veneboer, G. Puglisi, M. Mattia, D. Baker, S. C. Edwards, S. J. Edwards and P. J. Clarke. *Atmospheric models, GPS and InSAR measurements of the tropospheric water vapour field over Mount Etna*. *Geophysical Research Letters*, **29**(19): 1905, 2002. doi:10.1029/2002GL015159.

[Webley et al., 2002] P. W. Webley, R. M. Bingley, A. H. Dodson, G. Wadge, S. J. Waugh and I. N. James. *Atmospheric water vapour correction to InSAR surface motion measurements on mountains: results from a dense GPS network on Mount Etna*. *Physics and Chemistry of the Earth*, **27**: 363–370, 2002. doi:10.1016/S1474-7065(02)00013-X.

[Wegmüller et al., 2010] U. Wegmüller, D. Walter, V. Spreckels and C. L. Werner. *Nonuniform ground motion monitoring with TerraSAR-X persistent scatterer interferometry*. *IEEE Transactions on Geoscience and Remote Sensing*, **48**(2), 2010. doi:10.1109/TGRS.2009.2030792.

[Werner et al., 2003] C. Werner, U. Wegmüller, T. Strozzi and A. Wiesmann. *Interferometric point target analysis for deformation mapping*. *Proceedings of International Geoscience and Remote Sensing Symposium 2003 (IGARSS'03), Toulouse, France, July 21–25*, **7**: 4362–4364, 2003.

[Wessel and Smith, 1998] P. Wessel and W. H. F. Smith. *New, improved version of the Generic Mapping Tools released*. *EOS Trans. AGU*, **79**(579), 1998.

[Wiley, 1954] C. A. Wiley. *Pulsed Doppler radar methods and apparatus*. Technical report, United States Patent, No. 3196436, 1954.

[Zebker and Goldstein, 1986] H. A. Zebker and R. M. Goldstein. *Topographic mapping from interferometric synthetic aperture radar observations*. *Journal of Geophysical Research*, **91**(B5): 4993–4999, 1986. doi:10.1029/JB091iB05p04993.

[Zebker and Villasenor, 1992] H. A. Zebker and J. Villasenor. *Decorrelation in interferometric radar echoes*. *IEEE Transactions on Geoscience and Remote Sensing*, **30**(5): 950–959, Sep. 1992. doi:10.1109/36.175330.

[Zebker et al., 1994] H. A. Zebker, P. A. Rosen, R. M. Goldstein, A. Gabriel and C. L. Werner. *On the derivation of coseismic displacement fields using differential radar interferometry: The Landers earthquake*. *Journal of Geophysical Research*, **99**(B10): 19617–19634, 1994. doi:10.1029/94JB01179.

[Zebker et al., 1997] H. A. Zebker, P. A. Rosen and S. Hensley. *Atmospheric effects in interferometric synthetic aperture radar surface deformation and topographic maps*. *Journal of Geophysical Research*, **102**(B4): 7547–7563, 1997. doi:10.1029/96JB03804.

About the author — *Tom Rune Lauknes* was born in 1977 in Kirkenes, Norway, and grew up in the town of Tromsø. In December 2004, he graduated with the degree of Cand. Scient. (M. Sc. equivalent) in physics from the University of Tromsø, Tromsø, Norway. Since 2005, he has been a Research Scientist with the Northern Research Institute Tromsø (Norut), Tromsø. From September 2007 to August 2008, he was a Visiting Researcher with the Radar Interferometry Group, Stanford University, Stanford, CA, USA. In March 2011, he defended the current PhD thesis, entitled "Rockslide Mapping in Norway by Means of Interferometric SAR Time-Series Analysis" at University of Tromsø, Department of Physics and Technology. His research interests include SAR and InSAR signal processing techniques applied to surface displacement monitoring, glacier movement detection, and ionospheric studies.

ISBN 978-82-8236-024-1